Accepted Manuscript

Enhancing model temperature estimations in shallow, turbid, coastal regions: Mobile Bay, Alabama

Harikrishnan Sreeshylam[1,2], Zhilong Liu[1,2], Brian Dzwonkowski[1,2], John Lehrter[1,2]

[1] Stokes School of Marine and Environmental Sciences, University of South Alabama, Mobile, AL, United States

[2] Dauphin Island Sea Lab, Dauphin Island, AL, United States

Highlights

- Attenuation models varied in performances for shallow, turbid water temperatures.
- A new approach was developed from a relationship between surface salinity and PAR.
- The best overall performance involved surface trapping of incoming solar radiation.
- The evaluation of synoptic variability revealed a seasonal pattern in model performance.
- Surface correction to the net heat flux improved all temperature results.

Abstract

Accurate estimation of water column temperature is vital for modeling physical and biogeochemical processes. A key process in the thermal dynamics of the upper ocean is the attenuation of solar radiation. In shallow-turbid coastal systems, spatially and temporally varying optical characteristics present challenges for commonly used attenuation parameterization schemes. This study investigates the dependency of temperature with a ROMS model of Mobile Bay, a shallow, turbid estuary, using six different attenuation approaches including three base cases: Conventional approach PS77 based on water type-9; Novel approach SAL relating in situ PAR attenuation to salinity; and Surface trapped irradiance method ST. In addition, these base cases are also tested with surface atmospheric heat flux correction (QC). Simulations were validated against

observations from various sources to identify the optimal approach at annual and synoptic scales. While all simulations showed effective temperature performance over an annual cycle, monthly analysis revealed some seasonality, with winter months typically performing better than summer months. The influence of QC notably enhanced temperature performance in both annual and synoptic scales, given that surface heat flux primarily drove temperature changes in this shallow system. The best overall performance was determined to be the ST approach incorporating QC. Conversely, PS77 without QC demonstrated the poorest performance. The SAL model with QC, notably improved performance over PS77 with QC, yet demonstrated comparable yet weaker performance compared to the ST model with QC. The study also implies that neglecting subseasonal validation in long-term regional climate modeling could introduce uncertainty into analyzing events tied to subseasonal temperatures.

Keywords: ROMS, Solar attenuation, Temperature, Turbidity, Salinity, Heat flux, Shallow estuary

1. Introduction

Modeling efforts are rapidly advancing for coastal ecosystems, with temperature emerging as a state variable of critical importance. Precise estimation and modeling of temperature are paramount in investigating and predicting hydrodynamical and biogeochemical processes in coastal environments. Moreover, integrating hydrodynamical and biogeochemical models requires improved temperature simulations as the rate of biogeochemical processes approximately doubles per 10°C change in temperature (James, 1953; Hegarty,1973; Tjoelker, 2001). A fundamental control on the temperature is the penetration of solar radiation through the water column, which decreases exponentially with depth (Denman, 1973). The extent of this depth-dependent absorption of solar radiation is subject to variations influenced by the optical characteristics of the water column, which involve interactions with particulate and dissolved constituents. These interactions are particularly pronounced in coastal water bodies, highlighting the direct impact of water clarity on solar radiation absorption and, consequently, the vertical temperature distribution within the water column (Dake and Harleman, 1969; Zaneveld et al., 1981; Kara et al., 2004, 2005a, 2005b).

To account for the impact of water clarity, Jerlov (1976) proposed an optical classification system, categorizing seawater into nine types based on water clarity, primarily determined by the

amount of particulate and dissolved matter present. Ranging from clear open ocean water (Type I) to turbid coastal water (Type 9), each type is associated with distinct attenuation coefficients that characterize the optical properties governing the attenuation of light in seawater. The penetration of solar radiation into the water column decreases with increasing water type number. Utilizing the empirical attenuation coefficients of Jerlov's seawater types, Paulson and Simpson (1977, hereafter referred to as PS77) developed an improved parameterization of attenuation by using a double exponential formulation, one for shortwave wavelengths and one for infrared wavelengths. This formulation is widely used in community ocean models such as the Regional Ocean Modeling System (ROMS, Shchepetkin & McWilliams, 2005) to parameterize the attenuation of solar radiation and subsequent water column temperature. However, this formulation simplifies the transmission of solar radiation by employing exponential functions that rely on a single optical water type. This simplification fails to adequately capture the heterogeneous nature of the coastal ocean environment, where spatially variable optical properties are observed across salinity gradients and different estuaries (Schaeffer et al. 2011; Le et al. 2015; Liu et al., 2021). This shortcoming of the model underscores the need for a more flexible approach that can better represent the transmission process.

In this regard, a more precise vertical distribution of solar radiation in oceanic environments was developed with Inherent Optical Property (IOP) based optical models. This model accounts for spatial variations in optical properties, considering the differences in attenuation coefficients. Lee et al. (2005, referred to as Lee05) developed such a model based on observed absorption, and backscattering coefficients, which are adequately obtained through satellite ocean color remote sensing. This availability enables Lee05 to effectively quantify solar radiation transmission across various ocean water types, each with its distinct optical properties. However, this model tends to underestimate solar radiation transmission in coastal waters characterized by a high proportion of colored dissolved organic matter (CDOM) or total suspended sediments (TSS) (Zoffoli et al., 2017). Moreover, the inaccurate assumption of uniform IOP distribution throughout the water column underestimates subsurface attenuation in stratified conditions (Xing et al., 2020). Consequently, accurately predicting the entire photosynthetically active radiation (PAR) profile becomes challenging when relying solely on sea-surface IOP information obtained from ocean color remote sensing data.

Another significant challenge for accurately determining water temperature in coastal regions using common numerical approaches arises from excessive heating in shallow water. This issue typically stems from the interpolation of coarse forcing data into high-resolution coastal model grids, leading to deviations in temperature simulations (Ji et al., 2015). To mitigate the excess heating in the coastal water column, a practical data assimilation method of the model called "Q-correction" (referred to as QC) is employed. The QC technique involves a rapid correction of the net heat flux component of the atmospheric forcing conditions on the ocean surface, aiming to rectify the errors in the spatial mismatch between the meteorological forcing field and model grid (Barnier et al., 1995; Hetland and DiMarco, 2012; Zhang et al., 2012; Ji et al., 2015). The QC method effectively reduces errors by inserting the observed SST information into the primitive temperature transport equation to adjust the net heat flux at the surface. This incorporation introduces the information of actual observed data into the model. A detailed description of this approach is given in method section 3.2.4.

Based on these previous findings and considering the many factors influencing temperature simulations of coastal waters, this study investigated the impact of existing and novel attenuation parameterization methods on temperature simulations in a shallow, turbid marine system. The study area is Mobile Bay in the northern Gulf of Mexico, a shallow, river-dominated estuarine system where optical properties are spatially and temporally varying (Le et al. 2015). This study evaluates the efficacy and accuracy of six different modeling approaches for light attenuation in Mobile Bay by employing year-long simulations of the Regional Ocean Modeling System (ROMS). In addition to the existing conventional methods (e.g., PS77 and surface trapping of solar attenuation), a novel attenuation parameterization algorithm based on surface salinity is introduced (This method is referred as SAL hereafter). In this approach, surface salinity is used as a proxy for CDOM and TSS following the expectation of Xu et al. (2005). By conducting simulations with diverse attenuation parameterization approaches, this study aims to identify methods for improving the efficacy of model-based temperature estimations in shallow, turbid coastal waters under annual and subseasonal time scales. The attenuation approaches and validation methods are explained in section 3. Temperature validation of these models with observations are detailed in section 4. Rationales for differences in performance of these approaches are discussed in section 5.

2. Study Site

Mobile Bay is a wide, shallow drowned-river valley estuary on the northern Gulf of Mexico (Fig. 1). The bay is large, extending 48 km in length with a maximum width of 39 km. The deepest sections are concentrated within the dredged shipping channel, reaching a depth of nearly 16 m, while the average depth across the bay is approximately 3 m. Characterized as a micro-tidal estuary, Mobile Bay is predominantly influenced by river inputs, specifically from the Alabama and Tombigbee rivers, within an extensive drainage basin covering an area of 115,467 km^2 (Quinn et al., 1989). Notably, this river network generates the fourth largest streamflow in the United States (Swann et al., 2008). The annual mean river discharge into Mobile Bay amounts to 1866 $m^3 s^{-1}$ (Dykstra and Dzwonkowski 2021), with peak flow occurring from December to May and reduced flow conditions prevailing from June to November. It is worth highlighting that the river discharge serves as the primary source of material influx to the bay (Schroeder et al., 1990), significantly influencing the temperature, salinity, CDOM, and total suspended sediments within the estuarine system (Le et al. 2015).

Mobile Bay exhibits a high degree of turbidity, as indicated by an average Secchi disk depth of 0.8 m over a three-year sampling period (Rashleigh et al., 2009). The primary cause of turbidity in the bay is the presence of suspended sediments, which significantly contribute to light attenuation (Estes Jr et al., 2015). Additionally, river discharge introduces approximately 4 million metric tons of sediment into Mobile Bay each year, with nearly 70% of this sediment input occurring during the spring season (Ryan and Goodell, 1972). During spring, characterized by high river discharge, the bay displays spatially varying turbidity, with the northern region having higher levels and the southern bay having lower levels. During the summer season, minimal spatial variability in turbidity was observed, except for a distinct low signal in the mid-bay region. The fall season represented a transitional period, followed by a highly turbid winter period (La Violette et al., 1998), wherein winter wind events generated the most significant mixing power within this shallow system (Schroeder et al., 1990).

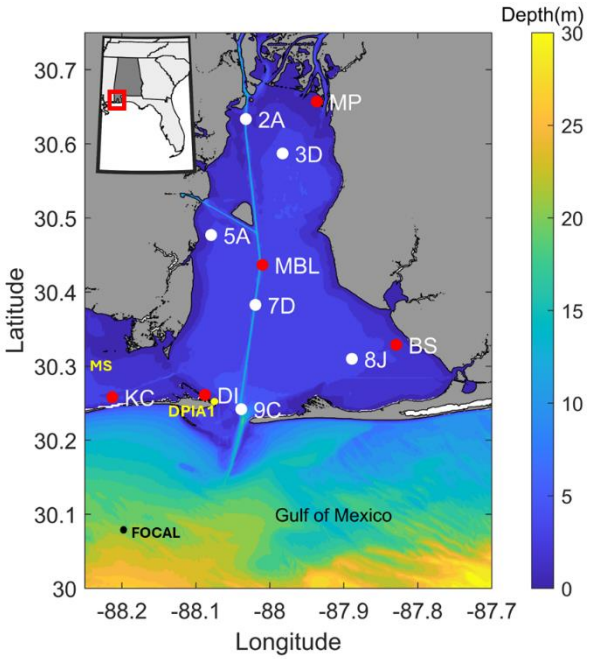

Fig. 1. Map of Mobile Bay with coloration representing the depth. Red circles denote fixed ARCOS stations while white circles represent selected CTD locations. Black dot on the shelf represents offshore FOCAL mooring station at 20m isobath. Inset map shows the bay location in U.S mainland.

Similarly, salinity in Mobile Bay experiences significant spatial and temporal variability. With the large river discharge and small tidal ranges, strong stratification is commonly observed throughout the bay (Schroeder et al. 1990; Ryan et al. 1997; Park et al. 2007; Kim and Park 2012; Coogan and Dzwonkowski 2018). During low discharge periods, strong stratification as high as 20 PSU m^{-1} in the pycnocline occurs in the bay (Coogan et al., 2020). In contrast, during periods of high discharge, the entire bay becomes predominantly freshwater-dominated and vertically mixed except for the deep ship channel, which remains stratified (Schroeder et al., 1990). The seasonal variability in discharge levels exerts a significant influence on the system, leading to reduced horizontal salinity gradients between the mouth and head during low discharge events and enhanced gradients during high discharge periods (Schroeder et al., 1990).

As such, the pronounced spatial and temporal variability in the optical and hydrographic conditions of Mobile Bay sets an ideal location for testing the performance of different attenuation parameterization methods on temperature simulations.

3. Methods

3.1. Model setup

A numerical model of Mobile Bay that has been previously developed and evaluated against observations of 2019 hydrographic data is used to test modifications to the solar attenuation parameterization. The model developed by Liu et al. (2022) used ROMS, and the domain includes the bay, delta, part of Mississippi Sound (MS), and the nearby coastal region (Fig. 1). The grid for this model was generated utilizing bathymetry and topography data sourced from the 1/3 arc-second NAVD 88 Coastal Digital Elevation Model of Mobile, Alabama (NOAA National Geophysical Data Center, 2009). This dataset included a horizontal resolution of approximately 8.87 m in the longitudinal direction and 10.27 m in the latitudinal direction. Supplementary information from 112 hydrographic surveys conducted between 2012 and 2019, accessible through the Army Corps of Engineers eHydro Survey Data portal, was also incorporated to enhance accuracy by including the recent bathymetric details for the Mobile River, Tombigbee River, and the shipping channel.

The model domain comprises 600 grid cells in the east-west direction, 840 grid cells in the north-south direction, and 16 layers in the vertical dimension, with near surface and near bottom refinement. A horizontally varying grid featuring a grid size of 70 - 90 m in the delta, shipping channel, and tidal inlets was used to address the intricacies of the system. In the open boundaries, this grid size gradually expands to 250 - 430 m. The wet/dry option was activated, enabling the consideration of truncated topography up to 1.0 m above sea level.

The model was subjected to hydrodynamic and meteorological forces. Tidal elevation, encompassing diurnal (K1, O1, Q1), semidiurnal (M2, S2, N2, K2), and over-tide constituents (M4, M6), was obtained from the Western North Atlantic, Caribbean, and Gulf of Mexico ADCIRC Tidal Databases. Open boundary conditions (western, southern, and eastern) were defined by hourly non-

tidal water level and currents, along with temperature and salinity data from the Northern Gulf of Mexico Operational Forecast System (NGOFS, Wei et al., 2014; Zheng et al., 2020). During 2019, the Bonnet Carré Spillway in the lower Mississippi River was extensively operated from Feb - Jul, resulting in significant increases in cumulative days of low salinity in the Western and Central Mississippi Sound. This event was shown to elevate the pressure forcing impacting the circulation in the bay (Wiggert et al. 2022). However, the NGOFS grid boundaries do not extend into the Lower Mississippi River, placing the Bonnet Carré Spillway outside the model domain and excluding it from the NGOFS forcing. River discharge at the closed northern boundary of Mobile Bay was determined by aggregating data from the Alabama River (USGS 02428400), Tombigbee River (USGS 02469761) and Satilpa Creek (USGS 02469800) stations. Meteorological forcing, including 3-hourly solar radiation, precipitation, wind, air temperature, sea surface temperature, and humidity, was sourced from the National Centers for Environmental Prediction (NCEP)'s North American Regional Reanalysis (NARR) data with 32 km spatial resolution. The conventional PS77 approach was utilized to parameterize solar attenuation within the model domain, utilizing coefficients of Jerlov's water type 9 specifically for turbid waters. The model implemented a net surface heat flux correction (QC) to eliminate differences between simulated sea surface temperature and prescribed sea surface temperature, as detailed in section 3.2.4 (Barnier et al., 1995).

This model simulation based on PS77 with QC-enabled attenuation scheme achieved a skill score of above 0.97 in temperature when compared with annual time-series observations of fixed long-term monitoring stations. However, it is crucial to acknowledge that the model's high skill in simulating temperature is primarily associated with the overwhelming annual signal over smallest subseasonal fluctuations, that are not well resolved. Additionally, validations with vertical hydrographic profiles also highlighted notable inconsistencies in the model's representation of vertical temperature distribution, suggesting the need for enhancements in the model temperature performance.

3.2. Model Simulations

To potentially enhance the temperature simulations utilizing this ROMS model, it is necessary to accurately parametrize the attenuation of solar radiation in the water column. This study considers three distinct base cases for attenuation parameterization: the conventional PS77 with water type-9 attenuation coefficients (PS77), a surface salinity-based attenuation (SAL) scheme, and a surface trapped irradiance (ST) method. The performances of these three methods are also tested with the surface atmospheric heat flux correction (QC) to facilitate additional refinement of the temperature simulations. The models were set up with a maximum time step of 3 s. A yearlong simulation was conducted for 2019, capturing hourly records of model outputs. The simulation began in November 2018, allowing for a two-month ramp-up.

3.2.1. PS77 with coefficients of Jerlov's water type 9

The conventional approach for parameterizing the attenuation in the water column using community ocean models such as ROMS utilizes the PS77 method. This method includes a three-parameter double exponential function to describe the penetration of irradiance through an optically homogeneous water column:

$$I_{(z)}/I_0 = R \cdot e^{z/\mu 1} + (1-R) \cdot e^{z/\mu 2} \quad (1)$$

where $I_{(z)}$ is the irradiance at a given depth z and I_0 is the net shortwave radiation at the surface. R is the empirical apportioning constant, μ_1 and μ_2 are the empirical vertical attenuation coefficients (m^{-1}), and these three empirical coefficients represent water clarity parameters and are determined from Jerlov's different seawater types (Jerlov 1976, Table XXVIII). These water types vary from clear ocean water to turbid coastal water. The first exponential term in equation (1) represents the attenuation in the surface layer due to the absorption of IR spectrum, while the second exponential stands for the attenuation of PAR in the deeper layers. For the model simulations of Mobile Bay and the surrounding area, the coefficients of Jerlov's type 9 were considered. This represents the absorption and penetration of downward irradiance in turbid coastal waters. This simplified approach of considering a constant attenuation coefficient through the entire model domain may not accurately capture the spatially and temporarily varying optical properties in coastal waters (Ko et al., 2016; Liu et al., 2021). This is likely true in Mobile Bay, a system characterized by turbidity,

where the optical characteristics of the water column display both spatial and temporal variability (La Violette et al., 1998).

3.2.2. Novel attenuation algorithm based on surface salinity

To account for the spatial and temporal variations in turbidity, a novel algorithm for parameterizing the attenuation is proposed by combining the ideas of Lee05 (Lee et al., 2005) and PS77. While the PS77 model fails to represent spatial variability in optical properties, Lee05 considers these variations, allowing for differences in attenuation coefficients and resulting in a more precise vertical distribution of solar radiation. Decomposing the total downward irradiance into visible (VIS, 350-700 nm) and infrared (IR, 700-2500 nm) bands, the Lee05 method defined the vertical transmittance as

$$I(z)/I_0 = F_{VIS} \cdot e^{K_{VIS}z} + (1 - F_{VIS})e^{K_{IR}z} \quad (2)$$

Where, F_{VIS} is the ratio of the visible portion to total irradiance with a general value of 0.47. K_{VIS} and K_{IR} are the diffuse attenuation coefficients varying with depth and sun angle for the visible and infrared portions, respectively. K_{VIS} also depends on inherent optical properties (IOP) of the water column. Combining Lee05 (Eq. 2) with PS77 (Eq. 1), a new attenuation scheme based on in-situ photosynthetically active radiation (PAR, 400 – 700 nm) measurement is proposed for shallow turbid systems like Mobile Bay. This scheme assumes that the infrared portion (> 700 nm) is absorbed by the surface layer, and uses an exponential function parameterizing the attenuation of PAR, given as

$$I(z)/I_0 = F_{PAR} \cdot e^{K_{PAR}z} + (1 - F_{PAR})\delta \quad (3)$$

Where K_{PAR} is the attenuation coefficient derived from hydrographic CTD data available in Mobile Bay and the adjacent shelf during April to September (stations are shown in Fig. 2a). F_{PAR} = 0.45 is the energy fraction of PAR in the total shortwave radiance. This value is derived from the ARCOS observations of PAR and solar radiation during April to September. δ is 1 in the surface layer and 0 in other layers. To consider the wide variation of K_{PAR} from the estuary head to the shelf, a regression analysis (Fig. 2b) between K_{PAR} and surface salinities leads to a new parameterization:

$$K_{PAR} = aS^b \quad (4)$$

When the surface salinity (S) approaches zero, the established correlation will become nonoperative. Consequently, the lower limit for salinity is rigorously defined as 0.001 psu. The coefficients a and b are 3.682 and -0.5017, respectively. This algorithm incorporates the attenuation of photosynthetically active radiation (PAR) resulting from the presence of CDOM and TSS in the water column. The surface salinity serves as a proxy for the CDOM or TSS concentration, taking into consideration the inverse relationship observed between salinity and CDOM or TSS concentration (Xu et al., 2005; Le et al., 2015). This new attenuation algorithm based on surface salinity (SAL) is implemented into ROMS for the second temperature simulation.

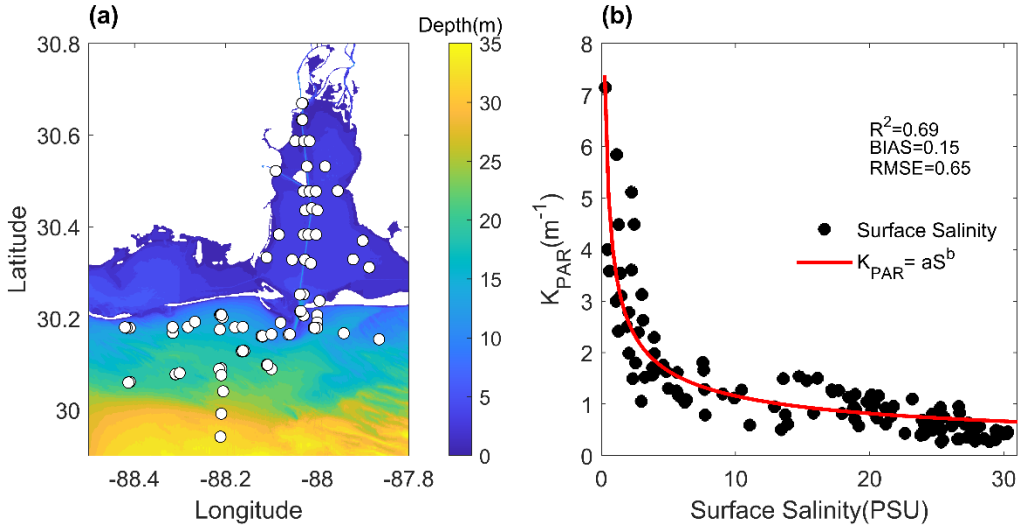

Fig. 2. (a) Map of Mobile Bay and adjacent coastal area showing CTD survey stations (white dots) from April to September 2019 with the coloration representing depth. (b) Non-linear regression analysis depicting the relationship between surface salinity (S) and PAR-derived attenuation coefficients at the CTD stations.

3.2.3. Surface trapped (ST) irradiance method

In the context of the shallow water column, a significant challenge encountered when employing the PS77 with water type 9 is the occurrence of excessive heating within the water column. This deviation of temperature simulation may be primarily attributed to the errors in net

ocean-atmosphere heat flux parametrization. Such heat flux errors in coastal sea areas may be caused by interpolating the coarse atmospheric forcing data into high-resolution model grids, as previously mentioned by Ji et al. (2015). The heat flux includes net short wave radiation that penetrates the water column, where the remainder (i.e., net heat flux minus shortwave) is absorbed in the surface-most layer. In a shallow system, if the penetration depth defined by water type 9 exceeds the water column depth, the remaining shortwave will likely be forced into the bottom vertical layer, resulting in increased warming at the bottom. This suggests that minimizing the role of shortwave radiation penetration may lower the water temperature in the underlying layers. This objective can be accomplished through the application of a surface layer trapping technique (referred as ST), which effectively prevents the penetration of short wave radiation into the water column. By incorporating such measures, the excessive heating experienced at the bottom layer can be potentially mitigated. In ROMS, this technique can be implemented by disabling the "SOLAR SOURCE" option during the conventional model setup. However, the adoption of this methodology may potentially lead to an increase in upper-layer temperature.

3.2.4. Base case simulations (PS77, SAL, ST) with heat flux correction (QC)

Interpolation of coarse resolution atmospheric forcing data into a model grid of fine resolution may cause deviations in model temperature simulations. In the models, the atmospheric forcing drawn from 3-hourly NARR data has a spatial resolution of 32 km while the model grid size varies horizontally from 70 - 90 m in the delta, shipping channel, and tidal inlet to 250 - 430 m towards the open boundaries. This suggests that the impact of this data interpolation may greatly affect the estuary compared to the shelf region. However, uncertainties could potentially be mitigated by employing a finer temporal resolution of atmospheric forcing. Nonetheless, the increased spatial variability between them is likely to remain a hindrance. To mitigate the expected issue of excessive warming resulting from the interpolation of coarse forcing data in the shallow water column during base simulations, a practical data assimilation technique known as Q-correction (QC) is employed in the subsequent simulations. The purpose of QC is to rectify errors in the meteorological forcing field by adjusting the net surface heat fluxes calculated by the atmospheric model before they are input into the ocean model. This method has been previously used and verified in many modeling efforts (e.g., Barnier et al. 1995, Hetland and DiMarco 2012,

Zhang et al. 2012, and Ji et al. 2015). The control equation governing the time evolution of ocean temperature at the surface is:

$$K_v \frac{\partial T}{\partial t} = \frac{Q_{NET}}{\rho_0 c_p} \quad (5)$$

Where K_v is the mixing coefficient that depend on depth; T is the ocean temperature; Q_{NET} is the net surface heat flux; ρ_0 is density; c_p is the specific heat. The net heat flux Q_{NET} is obtained by adding four components: shortwave solar radiation Q_S, longwave infrared radiation Q_{IR}, sensible heat flux Q_H and latent heat flux Q_E.

$$Q_{NET} = Q_S + Q_{IR} + Q_H + Q_E \quad (6)$$

The estimate of net surface heat flux during the time integration of ocean model can be written as:

$$Q_{NET}(T_S) = Q_{NET}\left(T_S^{clim}\right) + \left(-\frac{\partial Q_{NET}}{\partial T}\right)_{T_S^{clim}} \cdot \left(T_S^{clim} - T_S\right) \quad (7)$$

Where T_S is the model surface temperature and T_S^{clim} is the climatological sea surface temperature. The model's heat flux is expressed as the sum of two components: a prescribed climatological flux, which can be estimated using atmospheric reanalysis data like NARR, and the correction term (QC) proportional to the difference between the climatological SST and the model surface temperature. This correction term is estimated by determining the difference between the heat fluxes computed by the atmospheric model and the heat fluxes necessary to uphold observed ocean temperatures. This disparity is then applied to adjust the model's heat fluxes. The relaxation coefficient $\partial Q_{NET}/\partial T$ is derived from forcing data (NARR) using bulk formula (Barnier et al., 1995). This coefficient characterizes how surface heat flux varies in response to changes in the model ocean surface temperature over the climatological SST.

The influence of heat flux is quickly transmitted throughout the entire water column in the shallow water region, but its impact diminishes with increasing water depth since the QC cannot correct errors in the subsurface during model integration (Ji et al., 2015). Consequently, the QC method exhibits a more pronounced correction effect in coastal regions compared to deeper water areas, and model simulations that neglect this correction may lead to temperature estimation deviations in shallow regions. To implement the QC methodology, the "QCORRECTION" option

is enabled in the ROMS base setups. This option is utilized in conjunction with three base simulations to test the impact of this correction process.

3.3. Validation of temperature simulations

Validation involves temperature simulations at annual and synoptic (month to month) scales within the bay, focusing on the year 2019, a wet year with periodic low discharge conditions ideal for performance validation due to the system's varied discharge conditions (Fig. 3). These validations utilized temperature time series data from five real-time ARCOS (Alabama Real-Time Coastal Observing System) stations (DI, BS, MP, KC, MBL) across the bay shoals (Fig. 1), measured at approximately 0.5m above the bottom, with a temporal resolution of 30 min. Additional understanding of the behavior of different attenuation approaches and insight into the depth-dependent spatial variability was gained by examining the vertical temperature structure over channel and shoal locations. The vertical temperature validation utilized CTD measurements at three stations along the channel and three along the shoal of the bay (Fig. 1) from April to September, totaling 36 casts. This enabled separate analysis of the channel (18 stations) and shoal (18 stations) locations because of the very large depth difference between the sites. The sharp depth contrast between the channel (~14 m) and shoal (~3 m) may lead to performance variations between attenuation methods, necessitating careful examination. Additional insights into vertical temperature performances were gained by validating them against offshore FOCAL (Fisheries Oceanography in Coastal Alabama, Fig. 1) mooring temperatures at different depths. This offshore validation provides critical information on the performance of models outside the bay, which is critical considering the estuarine-shelf exchange performance of the models.

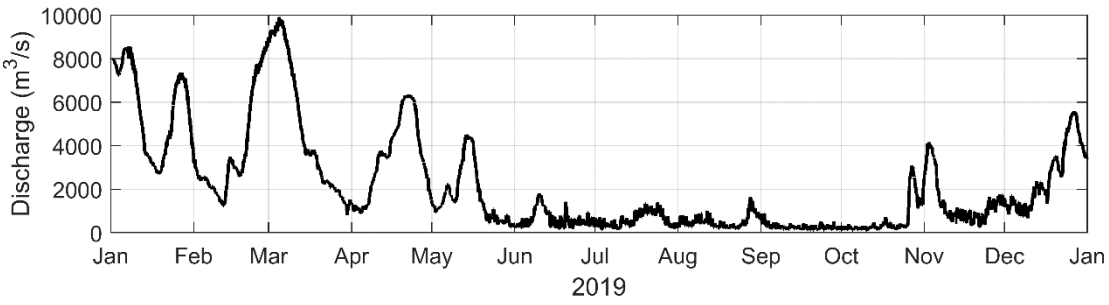

Fig. 3. Hourly river discharges into Mobile Bay for 2019 which was derived from the combined flows of the Alabama River, the Tombigbee River, and Satilpa Creek.

Simulated temperatures were validated against corresponding observations using metrics such as Root Mean Square Error (RMSE), bias, skill, and correlation coefficient (r).

$$RMSE = \frac{\sqrt{\Sigma_{i=1}^{N}(M_i - O_i)^2}}{N} \quad (8)$$

$$Bias = \frac{\Sigma_{i=1}^{N}(M_i - O_i)}{N} \quad (9)$$

$$Skill = 1 - \frac{\Sigma_{i=1}^{N}|M-O|^2}{\Sigma_{i=1}^{N}(|M-\bar{O}|+|O-\bar{O}|)^2} \quad (10)$$

$$r = \frac{\Sigma_{i=1}^{N}(M_i - \overline{M_i})(O_i - \overline{O_i})}{\sqrt{\Sigma_{i=1}^{N}(M_i - \overline{M_i})^2 \cdot \Sigma_{i=1}^{N}(O_i - \overline{O_i})^2}} \quad (11)$$

Where O and M are the observed and modeled data, respectively. The temporal average over the number of observations (N) is represented by the overbar symbol. The RMSE value provides an overall estimate of the prediction error, with lower values indicating better model performance (smaller errors between predictions and actual). Bias refers to the deviation or offset between the predictions and observed data, representing a consistent over-or underestimation by the model. Evaluating and reducing bias is crucial for enhancing the model's accuracy. Ideally, a bias close to zero indicates good agreement between the model and observed data. Skill acts as a global index of overall agreement between model and observation. A Skill value of 1 denotes perfect agreement, while 0 signifies complete disagreement between the model and observation. Pearson Correlation Coefficient (r) describes the strength and direction of the linear relationship between observation

and predictions. The correlation coefficient is meaningful only when there is a linear relationship between the two variables being analyzed. When this relationship is linear, the correlation coefficient accurately measures its strength. However, if the relationship is nonlinear, the correlation coefficient's usefulness diminishes or becomes questionable (Ratner, 2009). The values of r range from -1 (indicating a perfect negative correlation) to 1 (indicating a perfect positive correlation), with 0 showing no linear correlation. Values of r between 0.7 and 1 (-0.7 and -1) signify a strong positive (negative) linear relationship, indicating a solid linear rule. Values between 0.3 and 0.7 (-0.3 and -0.7) represent a moderate positive (negative) linear relationship, indicating a somewhat less consistent linear rule. Values between 0 and 0.3 (0 and -0.3) represent a weak positive (negative) linear relationship, indicating a very weak linear rule (Ratner, 2009).

Potential causes for weak model performance in the temperature time-series validations underwent further examinations by assessing the different forcing conditions expected to impact temperature simulations. Uncertainties in the atmospheric forcing of the model are assessed by validating the NARR-based forcing products with high resolution ARCOS-based atmospheric measurements across the bay and a NOAA NDBC station on Dauphin Island (DPIA1, Fig. 1). Meteorological observations by ARCOS are available at one minute sampling frequency, while NOAA NDBC has hourly measurements, both adjusted to a 10m height. Temporal resolutions of the observations were adjusted as necessary to match the hourly outputs of the model or the time step of the model forcing sources. The same performance metrics (i.e., Eqs. 8-11) were utilized in the assessments of the forcing.

4. Results

4.1. Yearly validations

Yearly validation of temperature simulations across all five ARCOS stations demonstrated a high level of performance in replicating the annual temperature pattern typical of subtropical systems. Several simulated cases are shown to highlight the overall quality of this annual performance across the five ARCOS stations (Fig. 4). A comprehensive assessment of the various model cases was achieved by aggregating annual performance metrics across the five ARCOS

stations (Table 1). When aggregated across ARCOS stations, all simulations exhibited RMSE values ranging from 0.75 to 1.16 °C, biases between 0.72 and 1.85 °C, and skill and correlation coefficients ranging from 0.95 to 0.98. Notably, among these annual validations, simulations incorporating QC exhibited favorable performance metrics compared to the base case simulations without QC.

Nonetheless, differences in performance metrics persisted even across QC-enabled simulations. Among the QC enabled simulations, the parameterization based on ST emerged as optimal, displaying the best combination of reduced RSME and bias, along with increased skill and correlation. Conversely, the conventional approach of PS77 without QC demonstrated the highest deviation from observations and had the least favorable validation metrics. In comparison to PS77 without QC, RMSE and bias in temperature improved by 42% and 87%, respectively, in the ST with QC approach. The novel surface salinity-based model (SAL and SAL with QC) exhibited performance levels between the extremes represented by ST with QC and PS77 without QC. The SAL (SAL with QC) approach outperformed PS77 (PS77 with QC) but lagged behind ST (ST with QC) method.

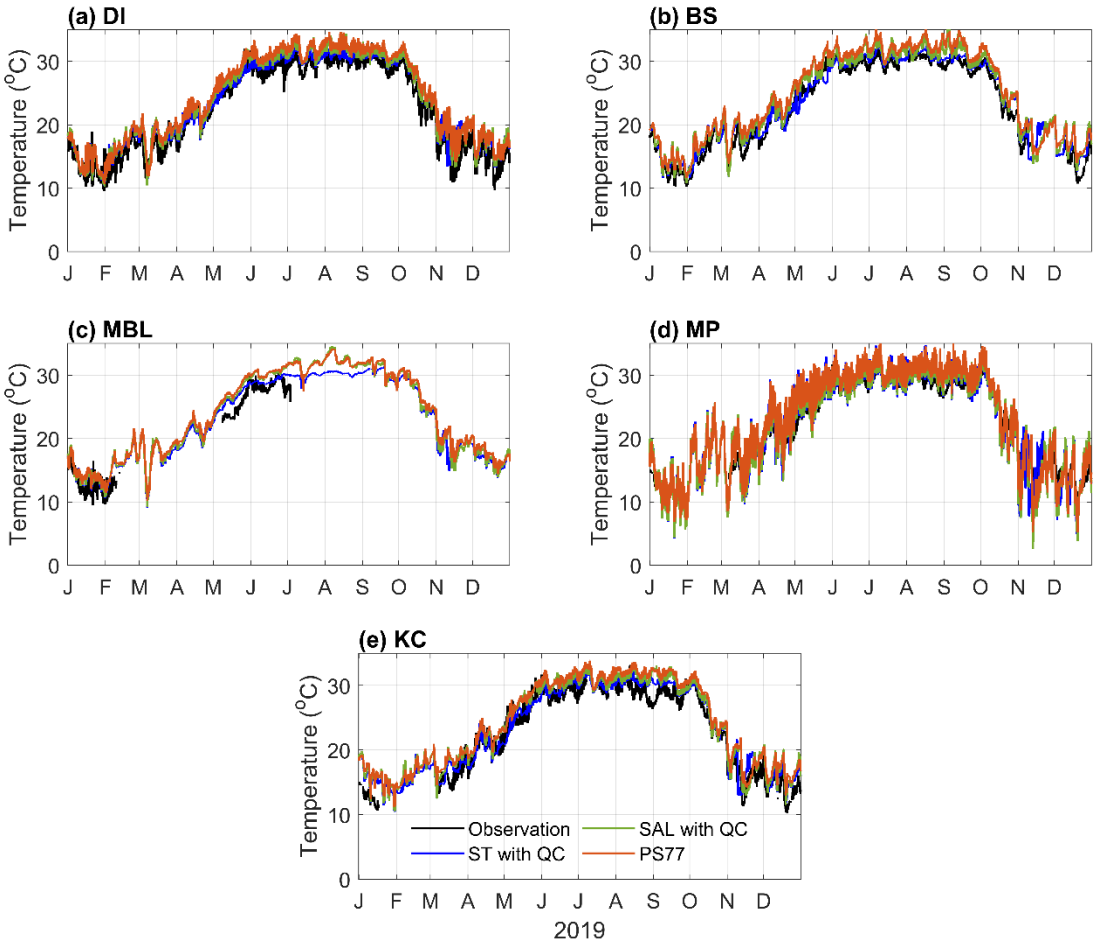

449 Fig. 4. Comparison between modeled and observed temperature time series during 2019 at five
450 ARCOS stations. The black line represents the observations, while blue, green, and red depict the
451 ST with QC (annual best), SAL with QC (salinity-based model), and PS77 (annual worst) based
452 temperatures, respectively. Remaining simulations can be found in supplementary materials: Fig.
453 S1, and statistical evaluations of individual stations are provided in supplementary materials: Table
454 S1.

Simulations	RMSE (°C)	Bias (°C)	Skill	*r*
PS77	1.16	1.85	0.96	0.95
PS77 with QC	0.95	1.14	0.97	0.97
ST	1.01	1.42	0.97	0.97
ST with QC	0.75	0.72	0.98	0.98
SAL	1.03	1.62	0.97	0.97
SAL with QC	0.89	0.86	0.98	0.98

Table 1. Statistical evaluation of temperatures simulated using six attenuation approaches for 2019. The values are derived from the aggregate of annual simulation at five ARCOS stations.

4.2. Synoptic scale performances

Despite favorable summary metrics at the annual timescale, a detailed inspection of the time series revealed notable deviations from observations in the synoptic scales across all simulations. This synoptic variability in performance is exemplified by a few simulated cases across multiple months at various ARCOS stations (Fig. 5). In these examples, the simulated temperatures exhibited notable deviations from observation highlighting the need for additional performance evaluation at the synoptic scale.

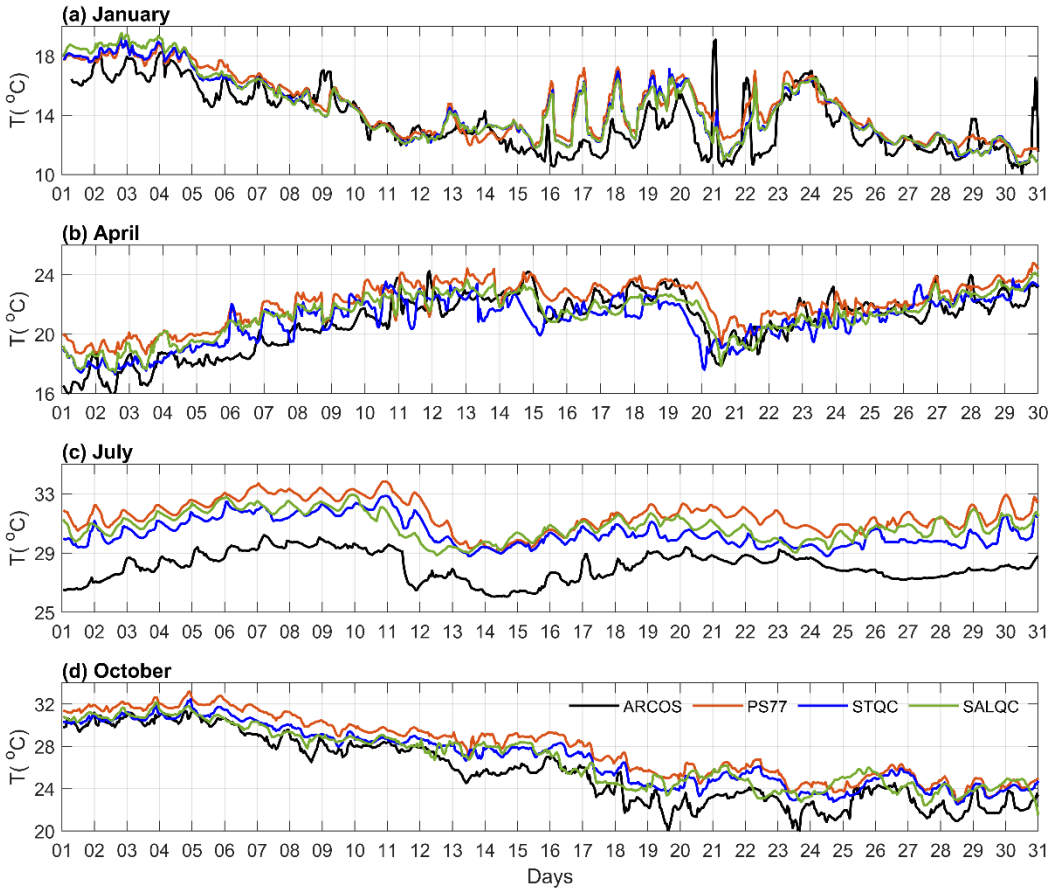

Fig. 5. Hourly time series comparison between observed and three selected modeled temperatures during (a) January (b) April (d) October at DI station and (c) July at KC station.

To better evaluate the ability of different light attenuation methods in capturing synoptic scale variability, monthly performance metrics were compiled across ARCOS stations. To highlight the patterns in the monthly performance metrics, several specific cases have been selected (Fig. 6). Over the course of the year, several individual months performed at levels similar to those seen in the annual evaluation. These higher performing months typically occurred in the winter, whereas summer months demonstrated weaker performance metrics. This was most apparent in the bias, skill, and correlation metrics. For example, in the PS77 case, the skill varied from 0.76 to 0.87 during winter months, while summer months showed variation between 0.48 to 0.57 (Fig. 6c). Similar seasonality was evident in the bias and correlation coefficient (Figs. 6b, d). Only RMSE

lacked a notable seasonal signal across most cases, although it displayed some signs of seasonality in the PS77 case (Fig. 6a).

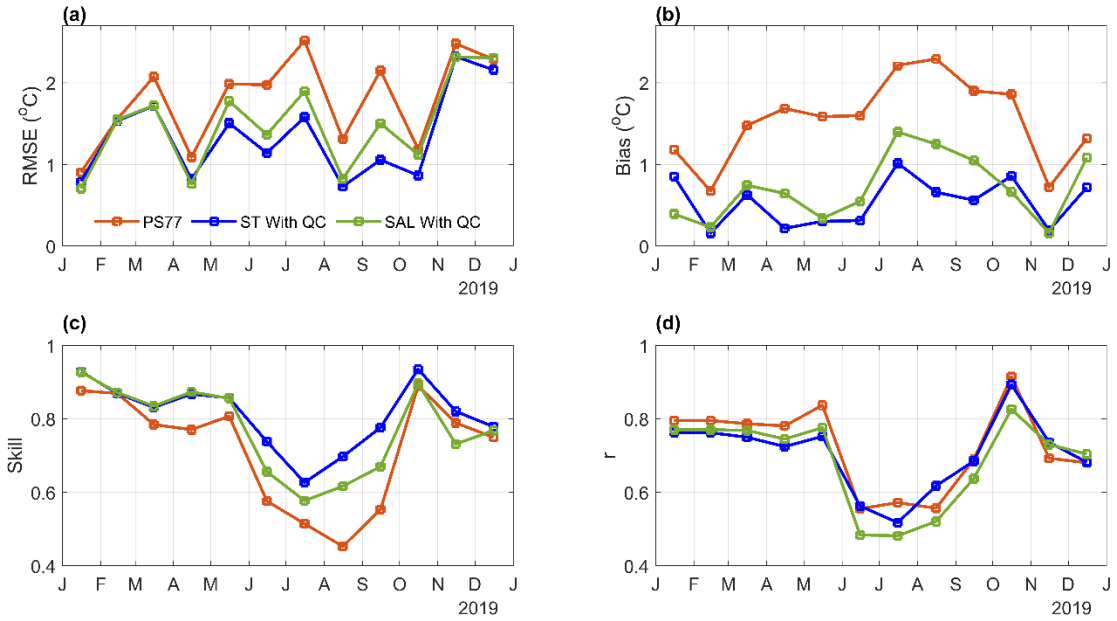

Fig. 6. Time-series comparison of monthly validation metrics between complied simulations and temperatures of ARCOS stations during 2019. Monthly comparisons of other simulations are provided in supplementary materials Fig. S2. Note these metrics were averaged across only four ARCOS stations (DI, BS, KC, MP) since data availability at MBL limit the ability to produce monthly statistics for some months.

It is important to note that simulations with QC exhibited the most favorable performance. While the magnitude of metrics such as RMSE, skill and bias favored QC enabled simulations, the correlation coefficient showed limited improvement from the base cases. Despite little separation in the correlation coefficient, the other performance metrics showed that both ST with QC and SAL with QC were generally the best performing cases across most months. Interestingly, there appeared to be a seasonality to the effectiveness of the QC, i.e. there was a bigger impact from QC in the summer months. This can be seen by comparing PS77 with the ST with QC and SAL with QC (Fig. 6). The monthly statistical metrics revealed QC during summer months reduced the RSME and bias by an average of nearly 45% across QC enabled simulations compared to those simulations

without QC. Conversely, during winter, the reduction in temperature metrics after implementing QC in simulations was <10%.

4.3. Validation of vertical temperatures

Examination of the vertical structure of the temperature simulations provided additional insights into the behavior of different attenuation approaches and the influence of QC. The initial examination of model cases at individual CTD stations in both the channel and shoals revealed a complex representation of the vertical temperature structure. Some simulations at channel and shoal stations were consistent with the observed vertical structure but exhibited notable bias from observations (e.g., Fig. 7a), while others demonstrated lower bias, but had differences in the vertical structure (Fig. 7b). However, some stations exhibited good fits between the model cases and observations (Figs. 7c, d). Considering the station-to-station variability in the vertical structure of simulations, aggregating the data from available months (Apr-Sept) provided a better understanding of the general performance of different cases.

The validation based on aggregated data of channel and shoals revealed consistency with the time series validations. Generally, ST with QC was the best performer, showing favorable metrics in reproducing the vertical temperatures, followed by SAL with QC (Table 2). Conversely, PS77 without QC showed the least favorable metrics. However, validation metrics of simulations exhibited increased deviations from observations in the channel, while shoals showed lower deviations. In the channel, all simulations showed RMSE values ranging from 2-2.8 ^{o}C, biases from 1-1.9 ^{o}C , and skill and correlation ranging from 0.67 to 0.89. In the shoals, the RMSE range was from 1.1-2 ^{o}C, bias from 0.7-1.8 ^{o}C, with skill and bias ranging from 0.88 to 0.97. Additionally, the influence of QC in enhancing the temperature prediction had varied effectiveness between channel and shoal. Relative to the base case simulations, QC-enabled simulations on the shoals experienced a reduction of up to 1 °C in RMSE and bias, whereas the channel sites showed a reduction of only approximately 0.60 °C.

Additional validation of offshore vertical temperatures using FOCAL mooring observations provided critical insights into bay-shelf connectivity performance. Offshore validations for the simulation year were conducted at surface (4 m), mid-depth (13 m), and bottom (18 m) depths

(Table 3). Similar to the bay performance, the ST with QC model demonstrated strong metrics in reproducing vertical temperatures at the shelf, followed by SAL with QC. Conversely, PS77 without QC showed the least favorable metrics. This decline in performance was evident at all depths, with RMSE increasing from 1°C to over 4°C, bias rising from 0.38°C to over 2.5°C, and skill and correlation dropping from 0.98 to 0.71 from surface to bottom. Additionally, the influence of QC in improving temperature prediction decreased with depth, from nearly 0.4°C improvement in RMSE and bias at the surface to <0.05°C at the bottom. The decline in performance with depth on the shelf suggests that the boundary conditions are likely more important on the shelf in deeper waters. Errors in the boundary conditions are likely leaking into the lower portion of the water column where the QC method is not effective at mitigating temperature error.

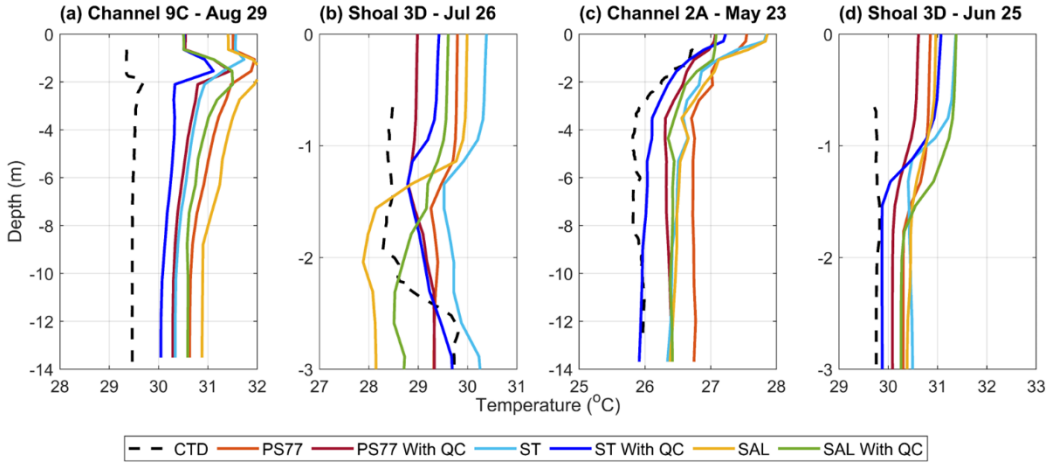

Fig. 7. Examples of the vertical temperature structure from observations and all the model cases at different channel (a, c) and shoal (b, c) locations within Mobile Bay including station 9C, 3D and 2A (see Fig. 1 for cast locations).

Simulations	(a) Channel Stations: 2A, 7D, 9C				(b) Shoal Stations: 3D, 5A, 8J			
	RMSE (ºC)	Bias (ºC)	Skill	r	RMSE (ºC)	Bias (ºC)	Skill	r
PS77	2.83	1.97	0.79	0.76	2.03	1.89	0.88	0.95
PS77 with QC	2.48	1.29	0.83	0.74	1.41	1.04	0.94	0.96
ST	2.76	1.77	0.8	0.88	2.01	1.71	0.88	0.97
ST with QC	2	1.08	0.89	0.86	1.11	0.77	0.95	0.96
SAL	2.78	1.83	0.81	0.8	1.91	1.87	0.89	0.96
SAL with QC	2.34	1.22	0.86	0.67	1.18	0.97	0.96	0.94

Table 2. Validation of vertical temperature simulations against vertical CTD temperatures of(a) channel and (b) shoals. The values correspond to the averages of validation conducted at three-channel stations and three shoal stations during Apr-Sept with one cast occurring per month.

Table 3. Validation of offshore temperature against (a) surface (b) mid-depth and (c) bottom temperatures of FOCAL during the simulation year 2019.

5. Discussion

5.1. Annual versus synoptic variability in performances

The temperature performance of different cases showed variability across different time scales, with notable changes in accuracy. The simulations consistently demonstrated effective temperature performance when evaluated over an annual cycle; however, there were notable fluctuations in accuracy when assessed on a monthly basis. Analysis of different cases at a monthly timescale revealed some seasonality in their temperature performance with winter months typically performing better than summer months.

The difference in performance at different evaluation time scales can be attributed to the dominance of annual temperature signal relative to synoptic scale fluctuations. Across all the ARCOS stations, there was a well define annual signal with a range of ~23°C typically spanned from 10°C to 33°C. By comparison, synoptic scale fluctuations varied across season within a range of approximately 10-20°C in winter, 13-30°C during spring, 27-34°C during summer and 17-34°C during fall (Fig. 4). These ranges were smaller than the annual signal. Therefore, the smaller synoptic scale fluctuations are overwhelmed by the well captured seasonal cycle of heating and cooling in the annual evaluation. By looking at monthly time scales, seasonal disparities in the ability of simulations to represent synoptic events were identified.

The seasonal differences in the representation of synoptic variability in water temperature are expected to be linked to the subseasonal quality of forcing conditions due to their connections to air-sea thermal interactions, circulation, and system hydrography. The primary air-sea interaction of interest is the net surface heat flux which plays a pivotal role controlling the thermal structure of water column (Edinger et al., 1968; Austin and Allen, 2011). In addition, thermal dynamics of Mobile Bay can also be influenced by circulation which is impacted by wind forcing (Schroeder et al., 1990; Park et al., 2007; Liu et al., 2022), promoting advective heat transport. Accurate heat transport by circulation thus depends on the fidelity of wind representation within the model. Both air-sea thermal interactions and circulation drive synoptic changes in the hydrographic structure of the water column, ultimately determining the system's thermal response to incoming heat and momentum fluxes (Garwood, 1979; Hendon, 2005).

Potential errors in the model's air-sea thermal interaction arise from net surface heat flux calculations (Eq. 6). Model-based net heat flux was estimated by incorporating components such as shortwave and longwave radiation data from hourly interpolated NARR. Estimation of latent and sensible heat flux uses atmospheric parameters, including air temperature, relative humidity, and wind speed data from NARR, along with water temperature from the model (ST with QC was used). These components were validated against ARCOS-based values, with latent and sensible heat fluxes solved using the COARE 3.5 algorithm (Edson et al., 2013). Due to the unavailability of upward shortwave and upward/downward longwave radiation data at the ARCOS stations, NARR data of those were used for observation-based heat flux estimations.

The subseasonal quality of atmospheric parameters and heat flux constituents influence net heat flux representation in the model, likely leading to seasonal variability in model temperature performance. Monthly average comparisons of hourly interpolated NARR parameters and heat flux constituents with ARCOS values are exemplified at station DI (Fig. 8). General agreement was seen in parameters such as air temperature, relative humidity, and wind speed, with some weakening in comparison during winter months (Fig. 8a,c,e). Latent and sensible heat flux estimations based on NARR values showed limited seasonality in performance, with a moderate increase in outflux compared to ARCOS values during the summer months (Fig. 8b,d). The downward solar radiation followed the annual patterns observed by ARCOS but exhibited an average bias increase of 55 W/m^2 over the year (Fig. 8f). This increase was notably higher from early spring to late summer. Such an increase in incoming solar radiation significantly impacts the net heat flux term, leading to an overprediction of net heat flux (Fig. 8g). This overprediction is modulated by the outgoing latent and sensible heat fluxes. The difference in net heat flux, primarily driven by discrepancies in shortwave radiation, can affect water temperature in a shallow system, as water temperature is more sensitive to changes in shortwave radiation than to air temperature during periods of increased solar radiation (Shinohara et al., 2021).

Using data from all available stations, a broader understanding of the sensitivity of model water temperature to net heat flux budget can be assessed. The aggregated performance bias and RMSE of each heat flux component and net heat flux across stations highlighted the contribution of different terms to the overall uncertainty in net heat flux (Fig. 9). The RMSE and bias of latent and sensible heat flux showed limited seasonality, with a bias range of less than 20 $W\ m^{-2}$, generally

favoring increased outflux during periods of heightened solar radiation. Downward solar radiation exhibited seasonally varying RMSE, with the highest values occurring in the summer months (Fig. 9a). The bias also followed this seasonality, averaging 59 W m^{-2} from spring to fall and peaking in the summer, while reaching 41 W m^{-2} in winter (Fig. 9b). This increase in the bias of downward solar radiation led to an increased bias in the net heat flux, with seasonal modulations driven by latent and sensible heat fluxes. The RMSE of net heat flux closely aligned with that of solar radiation, showing an increase of nearly 20 W m^{-2} in the summer compared to winter months. Their bias showed an average of 51 W m^{-2} in summer and 70 W m^{-2} in winter. This seasonality in the net heat flux performance by NARR leads to corresponding seasonality in the model water column temperature, as change in heat flux bias by 1 W m^{-2} could alter water temperature bias generally by up to 0.1 °C under warm water and weak wind conditions such as in summer, and by nearly 0.01 °C under increased wind stress and cold-water conditions of winter, on a monthly scale (Seager, 1989; Harrison, 1990; Cayan, 1991).

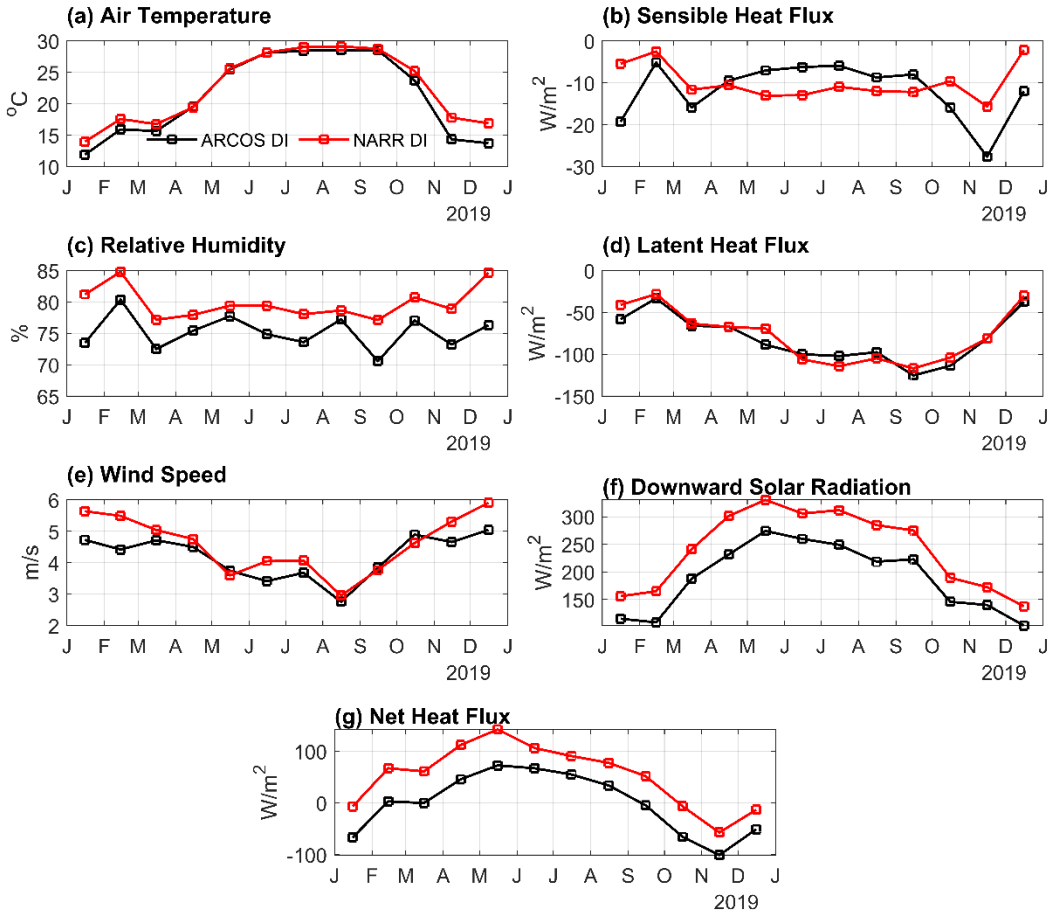

633 Fig. 8. Time series of monthly averaged meteorological parameters (a, c, e) and heat flux
634 components (b, d, f, g) obtained from DI ARCOS station (black) and corresponding NARR (red)
635 from hourly average data.

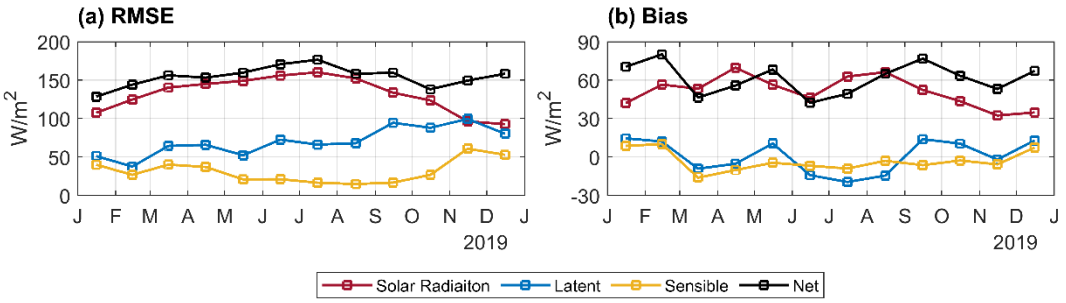

636 Fig. 9. Monthly RMSE and bias of heat flux components estimated from compiled values across
637 three ARCOS stations (DI, MP, KC). The BS station was excluded due to poor data quality. Note
638 that there was missing data at the considered stations; therefore, not all stations have the same
639 amount of data for a given month.

Another factor that can impact the thermal conditions in the bay is wind-driven circulation. While the magnitude of the wind forcing was relatively well captured as noted in the discussion on heat fluxes (e.g., Fig 8e) other aspects of the wind forcing, such as wind stress curl and wind direction can impact circulation. For example, wind stress curl generates vertical cyclonic (positive vorticity) and anticyclonic circulation (negative vorticity). A first order estimate of wind curl has been identified by pairing two along-bay stations DI and MP.

$$Curl_{MP,DI} = \frac{\tau_x(MP) - \tau_x(DI)}{\Delta y\ (MP,DI)} \quad (12)$$

Where τ_x is the north wind stress component and Δy is the distances between DI and MP stations. Assessing the subseasonal quality of wind curl involves comparing the hourly interpolated NARR based $Curl_{MP,DI}$ with that derived from observations, exemplified during January and July (Fig. 10). In these examples, the NARR generally agreed with observed curl signals but exhibited some limitations in capturing instantaneous large fluctuations in curl, particularly in January.

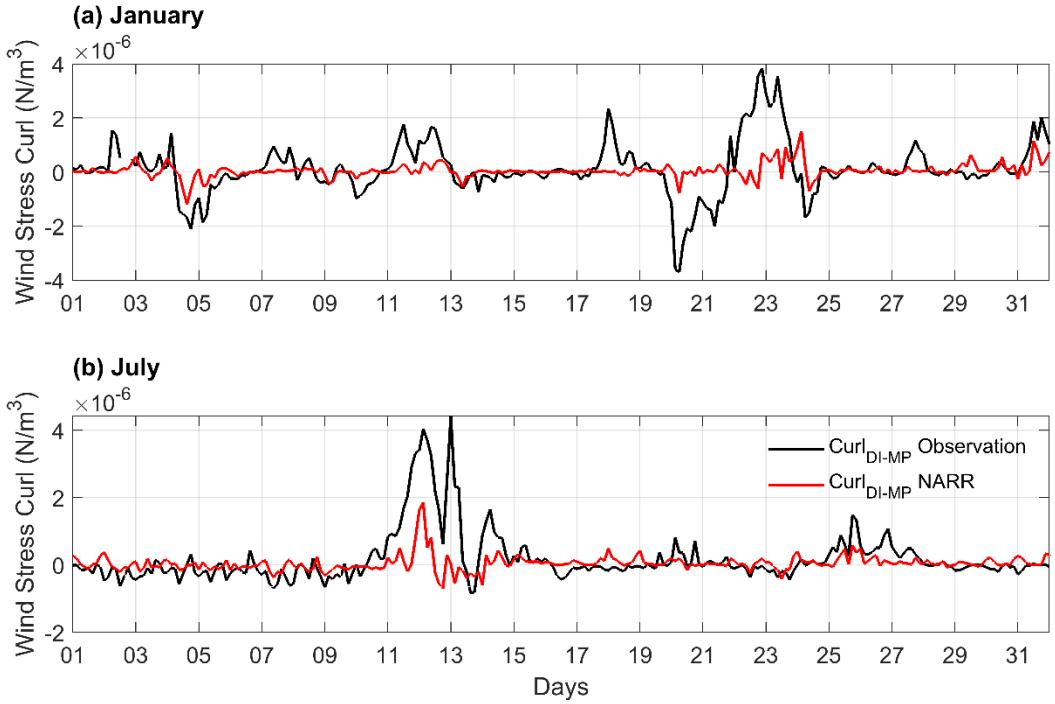

Fig. 10. Hourly averaged time series comparison of the NARR-derived wind curl (red) with observation-based estimations (black) during (a) January and (b) July.

Wind directionality and assessing its synoptic quality is expected to represent circulation impacts in the bay from diurnal sea-land breezes and upwelling/downwelling response along the coastline. Given the orientation of the system, North-South wind (*v* wind component) would capture sea-breeze/land-breeze diurnal signal, whereas East-West winds (*u* wind component) would capture the upwelling/downwelling signal, both may be able to drive thermal signals into the system. Assessing the subseasonal quality of wind direction involves comparing NARR-derived hourly interpolated u and v winds with observations from BS ARCOS station. This station was selected due to its location within the bay and its proximity to the mainland, where stronger land-sea breeze impacts are expected. Synoptic quality assessment of NARR's wind direction is exemplified by comparing the *u* and *v* winds against observations during January and July. Generally, NARR demonstrates agreement with observed wind signals, suggesting reliable representation of upwelling/downwelling (*u* wind) and sea-land breezes (*v* wind) conditions, with some uncertainty in capturing smaller temporal-scale events (Fig. 11). The NARR uncertainty decreased when wind directionality was validated at Dauphin Island (DI), a location somewhat isolated from stronger land-sea breeze effects, using wind observations from the NOAA NDBC (DPIA1) station (see supplementary materials Fig. S3). The improved performance towards the open boundary highlights NARR's limitations in accurately capturing diurnal wind signals in near-coastal areas, consistent with the findings of Lombardo et al. (2018) and Bouchard (2021). This uncertainty is likely to impact the model's ability to capture diurnal variability in temperature and circulation.

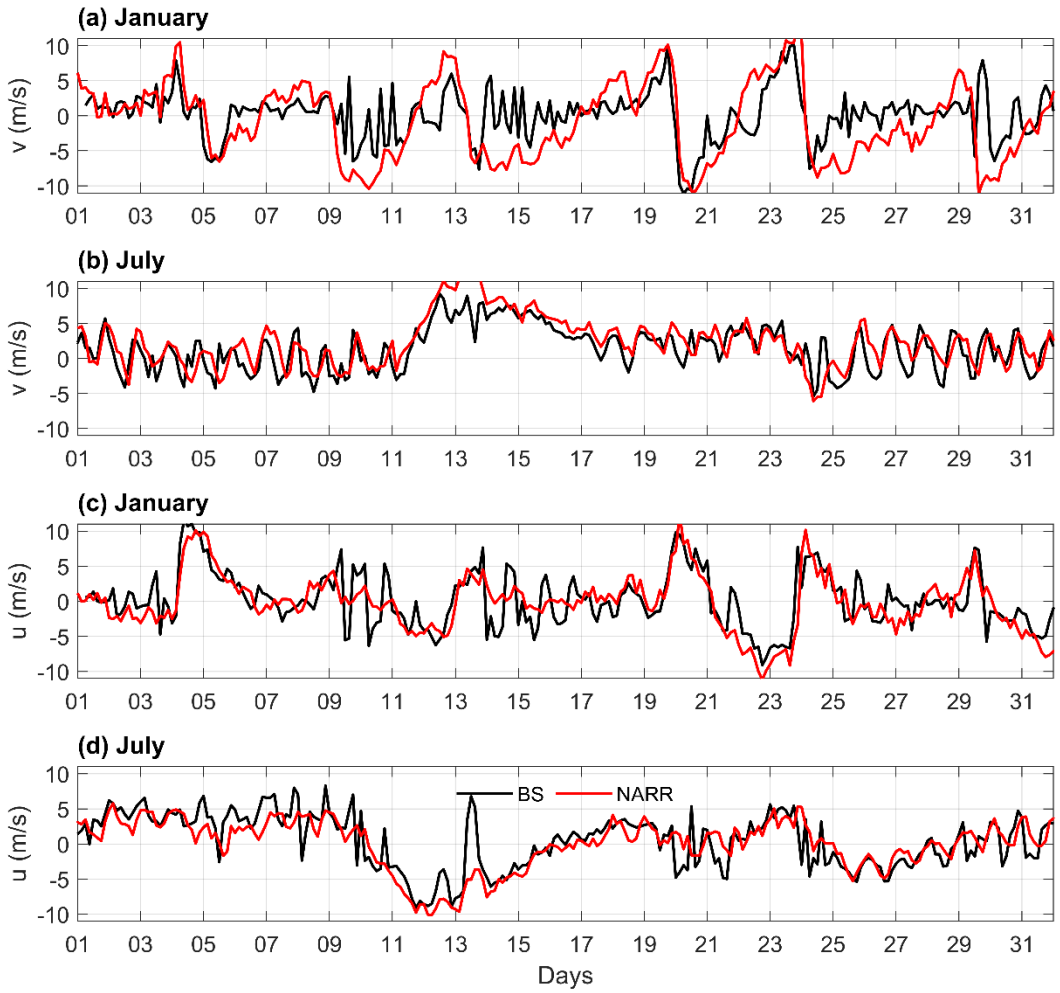

675 Fig. 11. Hourly averaged time series comparison of the NARR-derived u and v wind component
676 (red) to corresponding BS ARCOS measurements (black) during (a, c) January and (b, d) July.
677 Positive values of *u* (*v*) indicate eastward (northward) wind, while negative values indicate
678 westward (southward) wind.
679
680
681 In line with the examples, the monthly performance metrics of wind curl and directionality
682 generally showed agreement between NARR and ARCOS observations. Metrics of wind curl
683 yielded reliable results, especially RMSE and bias, suggesting seasonality in performance with
684 improvement in summer months compared to winter months (Figs. 12a, b), while skill and
685 correlation exhibited good values with limited seasonality (Figs. 12e, f). The diminished

representation of winter wind stress curl likely stems from challenges in capturing the intense wind gradients associated with cold front passages during non-summer seasons (Keen, 2002). However, periods when deviation occurred, as seen in Fig. 10, are not expected to be significant as the bottom stress curl due to the shallow depth of the system may limit the impact of vertical vorticity (Jia and Li, 2012). Similarly, examination of wind directionality also revealed a seasonality in performance. RMSE and bias of *u* and *v* winds show minor improvement in performance during summer months (Figs. 12c, d), while skill and correlation exhibit pattern without clear seasonality in quality (Figs. 12e, f). This modest summer enhancement may be attributed to intensified land-breeze/sea-breeze cycles in the region (Hill et al., 2010). Overall, the improved performance of NARR in summer wind dynamics contrasts with the decreased synoptic temperature performance. This contrast suggests that the seasonal variation in the model's wind-forced circulation is unlikely to be a significant contributor to the observed seasonal patterns in temperature performance.

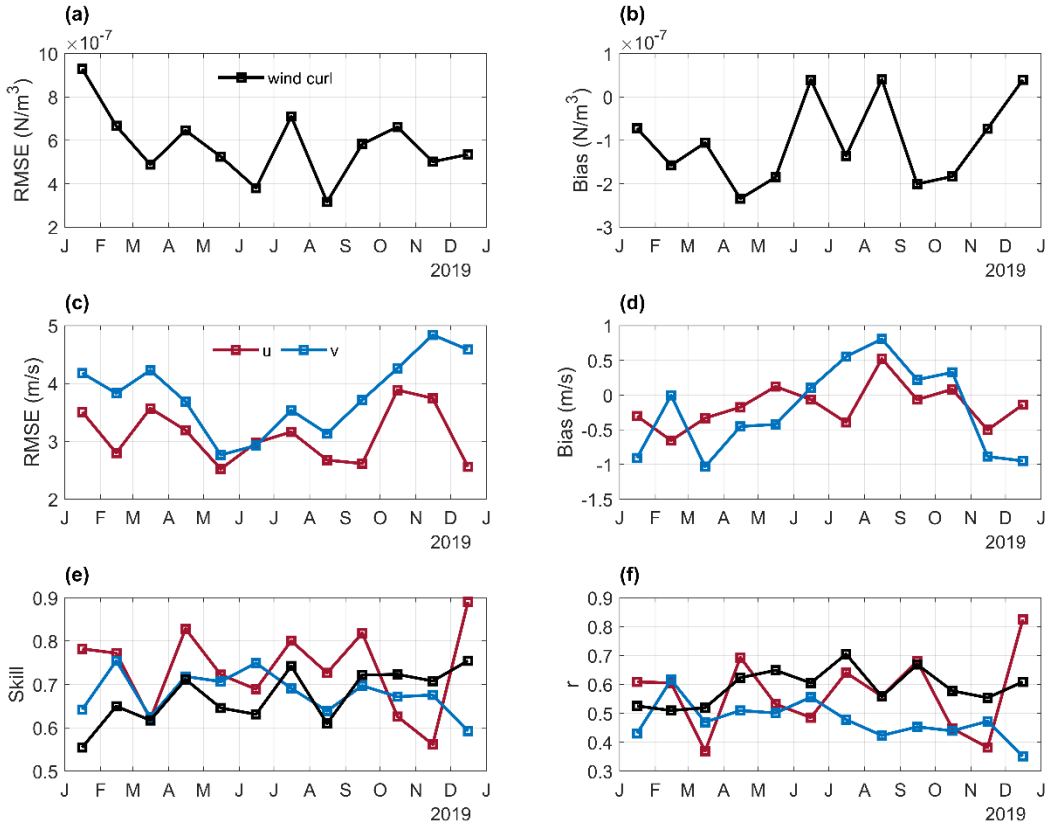

Fig. 12. Time-series comparison of monthly validation metrics of wind curl and directionality. The black line represents the metrics of curl estimated between MP and DI stations. The maroon and blue lines represent the BS ARCOS based monthly validation metrics of the *u* and *v* wind, respectively.

While the wind forcing conditions of the model demonstrate reliable synoptic performance, it is important to recognize that seasonal variations in wind forcing, along with corresponding atmospheric conditions, can significantly influence hydrographic conditions and thus the thermal structure of the system. Previous studies in lakes have noted that the seasonal thermal stratification has been associated with seasonal decrease in model performance (Beletsky and Schwab 2001; Beletsky et al., 2006; Austn and Allen, 2011; Beletsky et al., 2013). Therefore, examining seasonal changes in the hydrographic structure of the system is essential to determine whether they contribute to the degradation in synoptic-scale temperature performance.

The seasonal change in hydrography is influenced by atmospheric forcing conditions, primarily surface heat flux and wind-driven mixing. Generally, summer months are favored by positive net surface heat flux (Fig. 8g) enhancing heat content and potentially increasing thermal stratification in the system. The strong thermal forcing of the atmosphere couples with strong salinity stratification and weak wind to produce shallow mixed layers. On the other hand, winter months are characterized by negative net heat flux and diminished thermal stratification. This winter condition contributes to the destabilization of water column though enhanced heat loss and direct wind-driven mixing. However, in Mobile Bay, such conditions are in competition with salinity based restratification favored by river discharge, as identified by Coogan et al.(2020) based on long term observations at station MBL near the channel.

Examining the bay-wide seasonality in the model hydrographic conditions could contribute to explaining the seasonality in temperature performance of the model. The stratification was of particular interest and was represented by vertical salinity/temperature variance (Burchard and Rennau 2008; Wang et al. 2017; MacCready et al. 2018; Liu et al. 2022) as $S'^2 = (S - \bar{S})^2$ and $T'^2 = (T - \bar{T})^2$, where T and S are temperature and salinity respectively. $\bar{T}$ and $\bar{S}$ are depth averaged temperature and salinity, respectively. A system wide perspective of the spatial structure of the synoptic variability in hydrographic conditions is exemplified using the ST with QC model-based variance averaged in January and July (Fig. 13). Contrary to the expectations, both months exhibited weak thermal structure (Figs. 13a, b). Only the ship channel showed any notable thermal variance with some elevated values in January. However, there was notable salinity stratification with the highest values in the ship channel and deeper portions of the bay as expected. (Figs. 13c, d).

To better evaluate the synoptic variability in hydrography, hourly time series of bay-wide averaged temperature and salinity variance were examined (Figs. 13e, f). Temperature variance fluctuations showed no notable seasonal variability, but salinity fluctuations were more pronounced during summer compared to winter, likely due to occasional strong summer storms mixing the shallow water column (in contrast to the more persistent higher wind conditions in winter). To examine the potential seasonality in monthly hydrographic conditions in contributing to the seasonality in temperature performance of the model, the hourly variances were converted into monthly averaged values. The monthly average did not show seasonality in thermal stratification

744 (Fig. 13e), as the system stratification is mainly driven by salinity. In contrast, salinity variance
745 showed some seasonality, with limited enhancement in summer months compared to generally
746 diminished conditions in winter (Fig. 13f). Therefore, the bay-wide seasonal difference in salinity
747 stratification might also contribute to the seasonality of synoptic temperature performance of the
748 model, as the shallow mixed layers of summer can rapidly gain or loss heat (Miller, 1976).

749 The synergistic impact resulting from model degradation in air-sea thermal interactions and
750 alterations in the hydrographic structure likely contributed to the seasonal disparities observed in
751 the representation of synoptic variability in water temperature. The influence of these forcing
752 conditions on the seasonality in synoptic temperature performance is not clearly documented in
753 estuaries according to literature studies, which may be because temperature is generally a secondary
754 dynamical forcing and has not been a point of emphasis in some systems. For example, some early
755 numerical models of Mobile Bay did not simulate temperature yet were able to effectively capture
756 the main dynamics of the system (Kim et al., 2010; Kim and Park, 2012). With the more frequent
757 coupling of hydrodynamic and biogeochemical models in estuarine systems, there is a growing
758 need for improved temperature simulation in shallow highly stratified systems as biogeochemical
759 rates approximately double per change in temperature of 10°C (Q10 or Arrhenius rate expression).

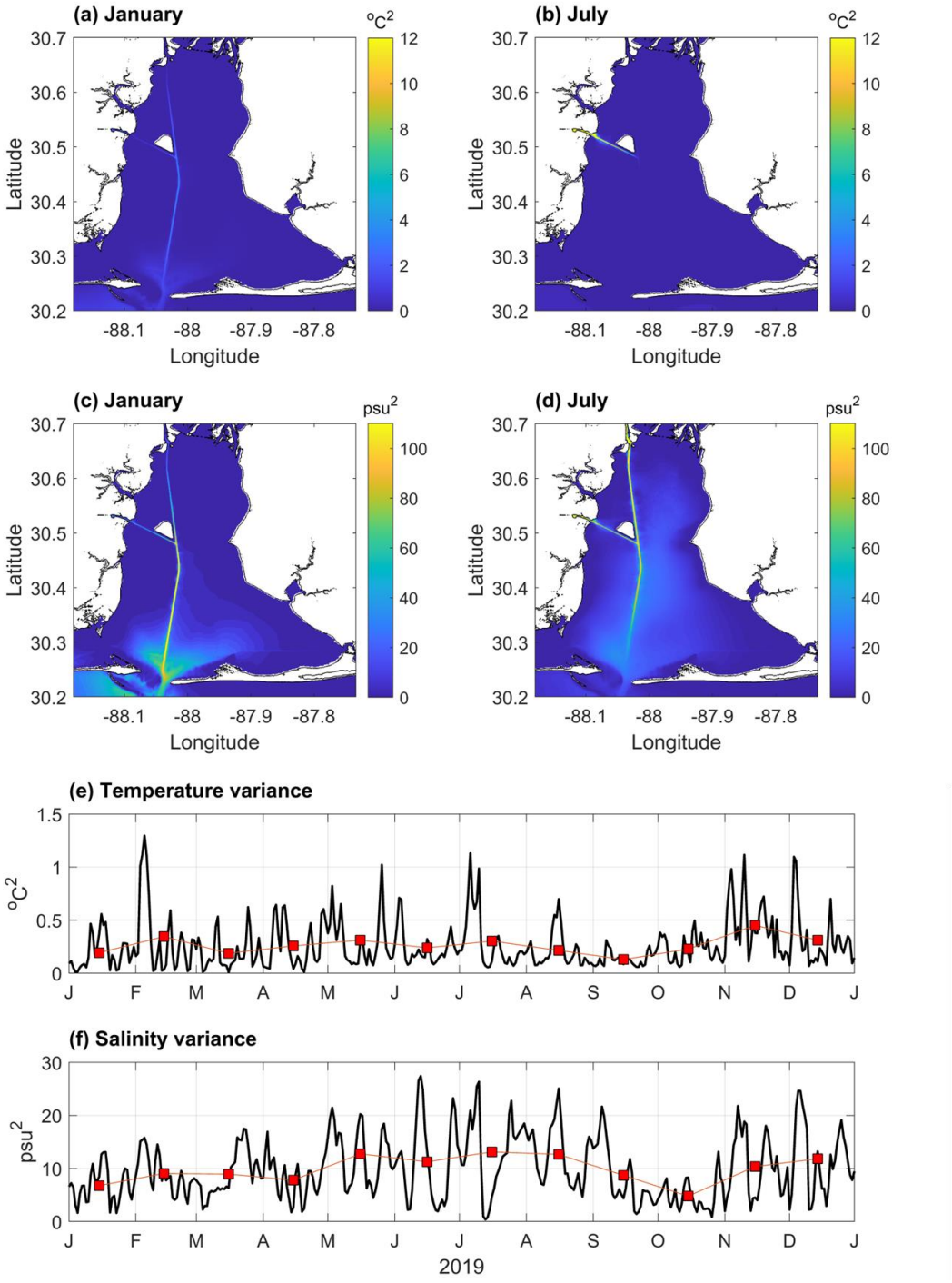

760 Fig. 13. Spatial patterns of depth averaged vertical (a, b) temperature variance ($\overline{T'^2}$) and (c, d)
761 salinity variance ($\overline{S'^2}$) defined using best performing ST with QC based model during January and
762 July. (e) and (f) show time series of the bay-wide temperature and salinity variances respectively,
763 with black line representing the hourly variance and blue squares representing their monthly
764 averages.

765

766

767 5.2. Influence of QC in simulations

768

769 While base case models tend to overheat the water column (i.e. bias is always positive, Table
770 1 and Fig. 6b), applying QC effectively mitigated temperature overpredictions, yielding more
771 realistic temperature estimates. This correction works at the surface, and it effectively drives a
772 reduction in temperature by adjusting the surface heat flux based on differences between the
773 modeled water temperature and atmospheric reanalysis temperature. The emphasis on heat flux at
774 the surface suggests that the shallow depth of the system may be an important feature that is key to
775 the improvement provided by the QC correction. The shallow depth of the system may limit the
776 importance of other terms in the heat budget so that the QC correction directly improves the most
777 important term in the heat budget of the system, i.e. surface heat flux.

778 To determine the relative importance of surface heat flux in the heat budget of the system a
779 simple one-dimensional (1D) heat budget analysis was conducted. A simple budget can be defined
780 as the change in depth-averaged temperature $\langle T \rangle$ that results from the change in the surface heat
781 flux Q_{surf} (Fewings and Lentz, 2011; Coogan et al., 2019).

782 $$\langle T_t \rangle - \langle T_{t=0} \rangle = \frac{1}{\rho_0 c_p h} \int_0^t Q_{surf}(t)\, dt \quad (13)$$

783 Where ρ_0 is the depth-averaged density, t is time, h is water depth, and Cp is the specific heat
784 capacity of seawater and equal to 3850 $J \cdot kg^{-1} \cdot C^{-1}$. The depth averaged changes in temperature
785 $(\langle T_t \rangle - \langle T_{t=0} \rangle)$ were calculated from the hourly time series of model temperature using ST with QC
786 at individual ARCOS station locations. Q_{surf} was estimated as the hourly interpolated time series
787 from NARR derived surface heat flux at these specific locations.

788 The equation has been solved at the locations of three ARCOS stations over the shoals (DI,
789 MP, KC) during the year. Station DI has been chosen as a representative example (Fig. 14) as all
790 the stations are generally similar in their results. These shoal sites generally followed Eq. 13,
791 suggesting that the surface heat flux is the dominant term driving the temperature change in this
792 shallow system. This also suggests that the model boundary condition limitations, such as those

from the Bonnet Carré Spillway opening, represent a secondary impact on simulated temperature in Mobile Bay. There was notable agreement between the temperature and 1D solution in summer months. In contrast, the winter showed modest deviations between the temperature change and the surface heat flux estimate. However , the terms in the 1D balance still closely followed each other (Fig. 14).

This provides insight into the effectiveness of QC in correcting model temperature performance. When the 1D balance is dominant, the heat flux is the primary source of temperature change, and QC directly impacts this component of the heat budget, significantly improving temperature simulations. Thus, in summer, QC is more effective at enhancing temperature simulations. In winter, where there are larger deviations from the 1D solution, QC is less impactful because it only operates on one of the terms contributing to the temperature budget. In such cases, the advection of heat would also be expected to contribute to the budget, as observed in this system at times (Coogan et al., 2019) and in other coastal systems (e.g., Fewings and Lentz, 2011).

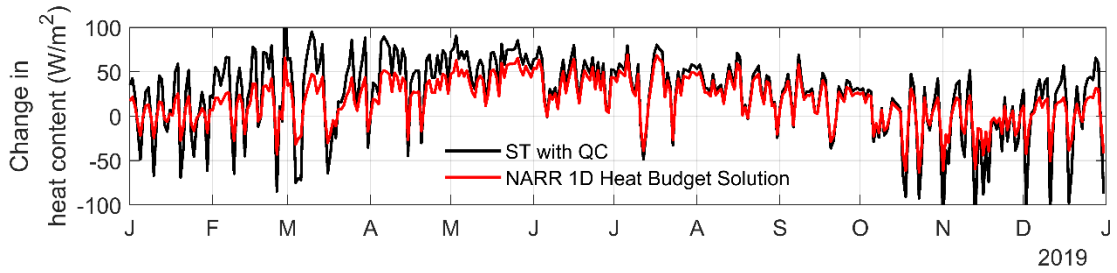

Fig. 14. Annual cycle of daily-averaged change in ST with QC based model heat content exemplified at location of ARCOS station DI (black) and corresponding 1D heat budget solution (red) based on NARR.

Interestingly, the effectiveness of QC varied depending on the attenuation approach used. In the surface-trapped attenuation method (ST), the QC correction acts to offset the impacts of surface-trapped irradiance, as both operate within the surface layer. Consequently, the adjustments made to the model temperature most directly address water column overheating. Conversely, the other two methods (SAL and PS77) distribute the heating throughout the water column according to their attenuation coefficient. This results in a certain degree of discontinuity between where QC

operates (at the surface) and where excess heating occurs (across the water column). Thus, it might be expected that QC is less effective in methods where incoming solar heating is distributed across the water column depth.

Additional aspects of the depth-dependency in the performance of QC also showed up in the vertical evaluation of the model performance in the bay and inner shelf. More pronounced correction by QC was seen in the shallower depths (bay shoals and shelf surface) compared to the deeper depths (bay channel and shelf bottom). This can be attributed to the increased impact of surface heat flux driving temperature signals in the shallow depths. On the other hand, the channel's role as a conduit for bay-shelf exchange likely introduced advective impacts that deviate from the 1D surface heat flux solution (Coogan et al., 2019), showing diminished effect of QC.

5.3. Influence of novel SAL-based model

Given the incorporation of in situ estimations of spatially and temporally varying salinity-based attenuation coefficients, it was anticipated that SAL (SAL with QC) model would outperform all other methods in simulating the temperature. However, the SAL (SAL with QC) method generally exhibited significant performance improvement only over the conventional PS77 (PS77 with QC) approach. Additionally, this method displayed comparable yet weaker performance in comparison to the overall best-performing ST (ST with QC) model upon the time series validation. This performance trend of the SAL method was also observed in the vertical validations of the temperatures at channel and shoal site.

The deterioration in the SAL approach from its anticipated optimal performance may be ascribed to several potential factors related to the formulation and evolution of the salinity-based attenuation algorithm. One possible limitation is fair weather bias in the in situ measurement of salinity and PAR profiles that were used to develop the algorithm. In this study, the in situ measurement of PAR profiles and salinity were carried out exclusively under weather conditions conductive to field work. This bias can have a substantial impact in this shallow river-dominated system where the combined forcing conditions of strong wind, tropic tides and moderate-to-high freshwater discharge can decouple the turbidity and salinity by sediment resuspension (Crozier and Schroeder, 1978; La Violette et al., 1999; Ha and Park, 2012). Other studies in shallow systems also

identified similar sediment resuspension that decouples with salinity (McKee and Baskaran, 1999; Liu and Huang, 2009). Such resuspension events may lead to substantial variations in light attenuation that are not synchronized with changes in salinity, consequently affecting the temperature estimations. Therefore, understanding the variability in turbidity with salinity is important in defining the light attenuation in a system such as Mobile Bay, where external forces drive increased turbidity signals. To further understand the potential of this methodology, additional field measurements across a broader spectrum of conditions and in diverse coastal systems are required.

Another possible limitation to the effectiveness of salinity-based attenuation parametrization is contingent on the model's ability to accurately simulate the surface salinity. The salinity performance of this model was evaluated by Liu et al., (2022) and showed broad range of skill values between ARCOS stations with scores ranging from 0.43 ~ 0.90. While the overall performance of salinity in the SAL cases is good (a skill of 0.88 upon ARCOS based validations), deviations in the model performance are nonetheless present. Consequently, errors in salinity modeling can act as a compounding factor, exacerbating inaccuracies in temperature estimations.

6. Conclusion

The accurate estimation of water column temperature stands as a crucial undertaking for ocean models of shallow-turbid coastal systems where commonly used solar radiation attention methods may have issues. In this study, the dependency of water temperature modeling on different parameterizations of solar radiation attenuation was explored. Using a ROMS model of Mobile Bay, six methods, including a new method that relates the PAR attenuation coefficient to surface salinity, were compared to in-situ observations to determine the best performance at annual and synoptic scales. All simulations consistently demonstrated effective temperature performance when evaluated over an annual cycle. However, analysis of different cases at a monthly timescales revealed some seasonality in temperature performance with winter months typically performing better than summer months.

Seasonal differences in synoptic water temperature variability were linked to the quality of model forcing conditions, with air-sea thermal interactions being the main source of uncertainty. Bias in net heat flux, mainly due to discrepancies in downward solar radiation, affected model sensitivity, causing greater temperature changes in the warmer, less windy summer conditions compared to colder, windier winter periods. Additional uncertainties arose from seasonal variability in hydrographic conditions; more pronounced summer salinity stratification may have influenced heat dynamics in shallow mixed layers. In contrast, wind performance showed strong agreement and improved accuracy in summer, suggesting that seasonal variation in wind-forced circulation is unlikely to significantly contribute to observed temperature performance patterns. Therefore, the combined impact of model degradation in air-sea thermal interactions and changes in hydrographic structure likely caused the seasonal disparities in synoptic water temperature variability.

Analyzing the performance of each base method over the course of a year showed that the ST method effectively mitigated overprediction and demonstrated proficiency in replicating temperature patterns in annual and synoptic scale. PS77's reliance on constant attenuation coefficients likely oversimplified the radiation transmission in this system. Despite the incorporation of in situ estimations of spatially and temporally varying salinity- based attenuation coefficients, the SAL method generally exhibited significant performance improvement only over the conventional PS77 approach, while displaying comparable yet weaker performance in comparison to the overall best-performing ST model. The decline in the SAL approach's performance may stem from limitations in its formulation and the bias in in situ measurements of salinity and PAR profiles, conducted only under fair weather conditions. This bias may be important in shallow river-dominated systems where sediment resuspension events, decoupling salinity and turbidity, lead to variations in light attenuation not synchronized with salinity changes, thereby affecting temperature estimations.

Enhancements were achieved in all three base parametrizations by incorporating a surface correction for the net heat flux using the practical data assimilation method QC. The effectiveness of QC was notable in both annual and synoptic time scales as the surface heat flux is the primary driver of temperature changes in this shallow system. The effectiveness of QC varied with the attenuation approach used. In the ST method, QC directly offsets surface-trapped irradiance impacts, addressing water column overheating within the surface layer. In contrast, the SAL and

PS77 methods distribute heating throughout the water column based on their attenuation coefficient, creating a discontinuity between where QC operates (at the surface) and where excess heating occurs (across the water column). Consequently, the ST method with QC proves more effective in preventing water column overheating and enhancing temperature estimation overall. This method is more convenient for modeling opaque water without considering downward irradiance. In systems where water column attenuation is known to be important, the SAL method that relates attenuation coefficient to surface salinity (SAL) combined with QC was encouraging.

This study implies that, even though temperature simulations achieved the highest accuracy on an annual scale, their synoptic scale variability should be considered to ensure the proper understanding of uncertainty in intraseasonal temperature-dependent events. For instance, uncertainties in defining the thermal structure during summer may impede the accurate representation of recurring hypoxic conditions, as the strong stratification and elevated water temperatures during this season contribute to hypoxic bottom waters in coastal systems. Additionally, the thermal structure and the associated heat content can contribute to the evolution of extreme weather events such as marine heatwaves and their impacts on ecosystems, e.g., coral bleaching. Analysis of such events, which are closely linked to summer temperatures, from long term regional 'climate' modeling simulations could be susceptible to unexpectedly high levels of uncertainty if the sub-seasonal validation is not considered. This may have notable impacts on understanding estuarine response to future climate scenarios. Foreseeing such impacts requires data assimilation and model uncertainty quantifications on a regional scale to ensure predictability.

Acknowledgments

This paper is a result of research funded by the National Oceanic and Atmospheric Administration's RESTORE Science Program under award NA19NOS4510194 to the University of South Alabama and Dauphin Island Sea Lab. This research was also possible due to support from the NOAA IOOS program via the Gulf of Mexico Coastal Ocean Observing System (NA21NOS120092). The authors would like to extend their appreciation to the Tech Support Group at the Dauphin Island Sea Lab for their continuous efforts in maintaining the Alabama Real-time Coastal Observing System. We are deeply grateful to Dr. Jeff Coogan at Coastal Monitoring

Alliance for his invaluable contribution in collecting the CTD data. Special thanks are extended to Dr. David Ralston, from Woods Hole Oceanographic Institution, for generously providing an early version of the ROMS Mobile Bay. We also thank Dr. Steve Dykstra at the University of Alaska Fairbanks for sharing the latest bathymetry data in the Mobile River, Tombigbee River, and the ship channel. We are deeply grateful to Dr. Lisa Lowe at North Carolina State University for High Performance Computing (HPC) support. The hydrodynamics modeling for this project was done on Expanse, at the San Diego Supercomputer Center (SDSC), through allocation EES210015 from the Advanced Cyberinfrastructure Coordination Ecosystem: Services & Support, which is supported by National Science Foundation grants #2138259, #2138286, #2138307, #2137603, and #2138296.

Data availability statement

The field data used for model validation can be accessed through the following link: https://arcos.disl.org. NOAA NDBC meteorological data at DPIA1 is accessed from https://www.ndbc.noaa.gov/station_page.php?station=dpia1. All data that were not downloaded from public sources have been made publicly available through the Dauphin Island Sea Lab Data Management Center (https://www.disl.edu/research/#dmc).

CRediT authorship contribution statement

Harikrishnan Sreeshylam: Conceptualization, Methodology, Resources, High performance computer model simulations, Investigation, Formal analysis, Validation, Visualization, Writing – original draft. Zhilong Liu: Model development, Conceptualization, Methodology, Writing – review & editing. Brian Dzwonkowski: Conceptualization, Resources, Supervision, Writing – review & editing, Project Administration. John Lehrter: Supervision, Writing – review & editing, Project administration.

968 References
969
970 Austin, J.A. and Allen, J., 2011. Sensitivity of summer Lake Superior thermal structure to
971 meteorological forcing. Limnology and Oceanography, 56(3), pp.1141-1154.

972 Barnier, B., Siefridt, L. and Marchesiello, P., 1995. Thermal forcing for a global ocean circulation
973 model using a three-year climatology of ECMWF analyses. Journal of Marine Systems, 6(4),
974 pp.363-380.

975 Beletsky, D. and Schwab, D.J., 2001. Modeling circulation and thermal structure in Lake
976 Michigan: Annual cycle and interannual variability. Journal of Geophysical Research: Oceans,
977 106(C9), pp.19745-19771.

978 Beletsky, D., Hawley, N. and Rao, Y.R., 2013. Modeling summer circulation and thermal structure
979 of Lake Erie. Journal of Geophysical Research: Oceans, 118(11), pp.6238-6252.

980 Beletsky, D., Schwab, D. and McCormick, M., 2006. Modeling the 1998–2003 summer circulation
981 and thermal structure in Lake Michigan. Journal of Geophysical Research: Oceans, 111(C10).

982 Bouchard, C., 2021. Exploring the Influence of Diurnal Forcing on Tidal Inlet Exchange and the
983 Impact on the movement of Oxygen Depleted Waters in the Mississippi Sound and Bight Region.

984 Burchard, H. and Rennau, H., 2008. Comparative quantification of physically and numerically
985 induced mixing in ocean models. Ocean modelling, 20(3), pp.293-311.

986 Cayan, D.R., 1992. Latent and sensible heat flux anomalies over the northern oceans: Driving the
987 sea surface temperature. Journal of Physical Oceanography, 22(8), pp.859-881.

988 Coogan, J. and Dzwonkowski, B., 2018. Observations of wind forcing effects on estuary length and
989 salinity flux in a river-dominated, microtidal estuary, Mobile Bay, Alabama. Journal of Physical
990 Oceanography, 48(8), pp.1787-1802.

991 Coogan, J., Dzwonkowski, B. and Lehrter, J., 2019. Effects of coastal upwelling and downwelling
992 on hydrographic variability and dissolved oxygen in Mobile Bay. Journal of Geophysical Research:
993 Oceans, 124(2), pp.791-806.

Coogan, J., Dzwonkowski, B., Park, K. and Webb, B., 2020. Observations of Restratification after a wind mixing event in a shallow highly stratified estuary. Estuaries and Coasts, 43, pp.272-285.

Crozier, G.F. and Schroeder, W.W., 1978. Mobile Bay turbidity study (No. NASA-CR-150711).

Dake, J.M. and Harleman, D.R., 1969. Thermal stratification in lakes: analytical and laboratory studies. Water resources research, 5(2), pp.484-495.

Denman, K.L., 1973. A time-dependent model of the upper ocean. Journal of Physical Oceanography, 3(2), pp.173-184.

Dykstra, S.L. and Dzwonkowski, B., 2021. The role of intensifying precipitation on coastal river flooding and compound river-storm surge events, Northeast Gulf of Mexico. Water Resources Research, 57(11), p.e2020WR029363.

Edinger, J.E., Duttweiler, D.W. and Geyer, J.C., 1968. The response of water temperatures to meteorological conditions. Water Resources Research, 4(5), pp.1137-1143.

Edson, J.B., Jampana, V., Weller, R.A., Bigorre, S.P., Plueddemann, A.J., Fairall, C.W., Miller, S.D., Mahrt, L., Vickers, D. and Hersbach, H., 2013. On the exchange of momentum over the open ocean. Journal of Physical Oceanography, 43(8), pp.1589-1610.

Estes Jr, M.G., Al-Hamdan, M.Z., Ellis, J.T., Judd, C., Woodruff, D., Thom, R.M., Quattrochi, D., Watson, B., Rodriguez, H., Johnson III, H. and Herder, T., 2015. A modeling system to assess land cover land use change effects on SAV habitat in the Mobile Bay estuary. JAWRA Journal of the American Water Resources Association, 51(2), pp.513-536.

Fewings, M.R. and Lentz, S.J., 2011. Summertime cooling of the shallow continental shelf. Journal of Geophysical Research: Oceans, 116(C7).

Garwood Jr, R.W., 1979. Air-sea interaction and dynamics of the surface mixed layer. Reviews of Geophysics, 17(7), pp.1507-1524.

Ha, H.K. and Park, K., 2012. High-resolution comparison of sediment dynamics under different forcing conditions in the bottom boundary layer of a shallow, micro-tidal estuary. Journal of Geophysical Research: Oceans, 117(C6).

Harrison, D.E., 1991. Equatorial sea surface temperature sensitivity to net surface heat flux: Some ocean circulation model results. Journal of climate, 4(5), pp.539-549.

Hegarty, T.W., 1973. Temperature coefficient (Q 10), seed germination and other biological processes. Nature, 243(5405), pp.305-306.

Hendon, H., 2005. Air-sea interaction. Intraseasonal Variability in the atmosphere-ocean climate system, pp.223-246.

Hetland, R.D. and DiMarco, S.F., 2012. Skill assessment of a hydrodynamic model of circulation over the Texas–Louisiana continental shelf. Ocean Modelling, 43, pp.64-76.

Hill, C.M., Fitzpatrick, P.J., Corbin, J.H., Lau, Y.H. and Bhate, S.K., 2010. Summertime precipitation regimes associated with the sea breeze and land breeze in southern Mississippi and eastern Louisiana. Weather and Forecasting, 25(6), pp.1755-1779.

James WO. 1953. Plant Respiration. Oxford, UK: Clarendon

Jerlov, N.G., 1976. Marine optics. Elsevier.

Ji, Q., Zhu, X., Wang, H., Liu, G., Gao, S., Ji, X. and Xu, Q., 2015. Assimilating operational SST and sea ice analysis data into an operational circulation model for the coastal seas of China. Acta Oceanologica Sinica, 34, pp.54-64.

Jia, P. and Li, M., 2012. Dynamics of wind-driven circulation in a shallow lagoon with strong horizontal density gradient. Journal of Geophysical Research: Oceans, 117(C5).

Kara, A.B., Hurlburt, H.E., Rochford, P.A. and O'Brien, J.J., 2004. The impact of water turbidity on interannual sea surface temperature simulations in a layered global ocean model. Journal of physical oceanography, 34(2), pp.345-359.

Kara, A.B., Wallcraft, A.J. and Hurlburt, H.E., 2005. A new solar radiation penetration scheme for use in ocean mixed layer studies: An application to the Black Sea using a fine-resolution hybrid coordinate ocean model (HYCOM). Journal of physical oceanography, 35(1), pp.13-32.

Kara, A.B., Wallcraft, A.J. and Hurlburt, H.E., 2005. Sea surface temperature sensitivity to water turbidity from simulations of the turbid Black Sea using HYCOM. Journal of physical oceanography, 35(1), pp.33-54.

Keen, T.R., 2002. Waves and currents during a winter cold front in the Mississippi bight, Gulf of Mexico: Implications for barrier island erosion. Journal of Coastal Research, pp.622-636.

Kim, C.K. and Park, K., 2012. A modeling study of water and salt exchange for a micro-tidal, stratified northern Gulf of Mexico estuary. Journal of Marine Systems, 96, pp.103-115.

Kim, C.K., Park, K., Powers, S.P., Graham, W.M. and Bayha, K.M., 2010. Oyster larval transport in coastal Alabama: Dominance of physical transport over biological behavior in a shallow estuary. Journal of Geophysical Research: Oceans, 115(C10).

Ko, D.S., Gould Jr, R.W., Penta, B. and Lehrter, J.C., 2016. Impact of satellite remote sensing data on simulations of coastal circulation and hypoxia on the Louisiana Continental Shelf. Remote Sensing, 8(5), p.435.

La Violette, P.E., Arnone, R.A. and Ladner, S., 1999. Space and time scales of optical variability in and about Mobile Bay as defined by a NOAA AVHRR visible sensor c660 algorithm. Continental shelf research, 19(3), pp.299-315.

Le, C., Lehrter, J.C., Hu, C., Schaeffer, B., MacIntyre, H., Hagy, J.D. and Beddick, D.L., 2015. Relation between inherent optical properties and land use and land cover across Gulf Coast estuaries. Limnology and Oceanography, 60(3), pp.920-933.

Lee, Z., Du, K., Arnone, R., Liew, S. and Penta, B., 2005. Penetration of solar radiation in the upper ocean: A numerical model for oceanic and coastal waters. Journal of Geophysical Research: Oceans, 110(C9).

Liu, X. and Huang, W., 2009. Modeling sediment resuspension and transport induced by storm wind in Apalachicola Bay, USA. Environmental Modelling & Software, 24(11), pp.1302-1313.

Liu, Y., He, R. and Lee, Z., 2021. Effects of ocean optical properties and solar attenuation on the northwestern Atlantic Ocean heat content and hurricane intensity. Geophysical Research Letters, 48(13), p.e2021GL094171.

Liu, Z., Lehrter, J., Dzwonkowski, B., Lowe, L.L. and Coogan, J., 2022. Using dissolved oxygen variance to investigate the influence of nonextreme wind events on hypoxia in Mobile Bay, a shallow stratified estuary. Frontiers in Marine Science, 9, p.989017.

Lombardo, K., Sinsky, E., Edson, J., Whitney, M.M. and Jia, Y., 2018. Sensitivity of offshore surface fluxes and sea breezes to the spatial distribution of sea-surface temperature. Boundary-layer meteorology, 166, pp.475-502.

MacCready, P., Geyer, W.R. and Burchard, H., 2018. Estuarine exchange flow is related to mixing through the salinity variance budget. Journal of Physical Oceanography, 48(6), pp.1375-1384.

McKee, B.A. and Baskaran, M., 1999. Sedimentary processes of Gulf of Mexico estuaries. Biogeochemistry of Gulf of Mexico Estuaries. Wiley, New York, pp.63-85.

Miller, J.R., 1976. The salinity effect in a mixed layer ocean model. Journal of Physical Oceanography, 6(1), pp.29-35.

Park, K., Kim, C.K. and Schroeder, W.W., 2007. Temporal variability in summertime bottom hypoxia in shallow areas of Mobile Bay, Alabama. Estuaries and Coasts, 30, pp.54-65.

Paulson, C.A. and Simpson, J.J., 1977. Irradiance measurements in the upper ocean. Journal of Physical Oceanography, 7(6), pp.952-956.

Quinn, H.A., Tolson, J.P., Klein, C.J., Orlando, S.P. and Alexander, C., 1989. Strategic assessment of near coastal waters. Susceptibility and status of Gulf of Mexico estuaries to nutrient discharges. Summary report.

Rashleigh, B., Cyterski, M., Smith, L.M. and Nestlerode, J.A., 2009. Relation of fish and shellfish distributions to habitat and water quality in the Mobile Bay estuary, USA. Environmental monitoring and assessment, 150, pp.181-192.

Ratner, B., 2009. The correlation coefficient: Its values range between+ 1/− 1, or do they? Journal of targeting, measurement and analysis for marketing, 17(2), pp.139-142.

Ryan, H.F., Noble, M.A., Williams, E.A., Schroeder, W.W., Pennock, J.R. and Gelfenbaum, G., 1997. Tidal current shear in a broad, shallow, river-dominated estuary. Continental Shelf Research, 17(6), pp.665-688.

Ryan, J.J. and Goodell, H.G., 1972. Marine geology and estuarine history of Mobile Bay, Alabama part 1. Contemporary sediments. Geological Society of America Memoirs, 133, pp.517-554.

Schaeffer, B.A., Sinclair, G.A., Lehrter, J.C., Murrell, M.C., Kurtz, J.C., Gould, R.W. and Yates, D.F., 2011. An analysis of diffuse light attenuation in the northern Gulf of Mexico hypoxic zone using the SeaWiFS satellite data record. Remote Sensing of Environment, 115(12), pp.3748-3757.

Schroeder, W.W., Dinnel, S.P. and Wiseman, W.J., 1990. Salinity stratification in a river-dominated estuary. Estuaries, 13, pp.145-154.

Seager, R., 1989. Modeling tropical Pacific sea surface temperature: 1970–87. Journal of physical oceanography, 19(4), pp.419-434.

Shchepetkin, A.F. and McWilliams, J.C., 2005. The regional oceanic modeling system (ROMS): a split-explicit, free-surface, topography-following-coordinate oceanic model. Ocean modelling, 9(4), pp.347-404.

Shinohara, R., Tanaka, Y., Kanno, A., Matsushige, K., 2021. Relative impacts of increases of solar radiation and air temperature on the temperature of surface water in a shallow, eutrophic lake. Hydrology Research 52(4), 916–926.

Swann, R., T. Herder, R. McElhenney, M. Hamilton, D. Yeager and L. Young, 2008. State of Mobile Bay: A Status Report on Alabama's Coastline from the Delta to Our Coastal Waters.

Tjoelker, M.G., Oleksyn, J. and Reich, P.B., 2001. Modelling respiration of vegetation: evidence for a general temperature-dependent Q10. Global change biology, 7(2), pp.223-230.

Wang, T., Geyer, W.R. and MacCready, P., 2017. Total exchange flow, entrainment, and diffusive salt flux in estuaries. Journal of Physical Oceanography, 47(5), pp.1205-1220.

Wei, E., Yang, Z., Chen, Y., Kelley, J.G.W. and Zhang, A., 2014. The northern Gulf of Mexico Operational Forecast System (NGOFS): model development and skill assessment.

Wiggert, J.D., Armstrong, B.N., Cambazoglu, M.K. and Kuttan, S.K., 2022. Mid-Breton Sediment Diversion (MBrSD) Assessment–Final Report.

Xing, X., Boss, E., Zhang, J. and Chai, F., 2020. Evaluation of ocean color remote sensing algorithms for diffuse attenuation coefficients and optical depths with data collected on BGC-Argo floats. Remote Sensing, 12(15), p.2367.

Xu, J., Hood, R.R. and Chao, S.Y., 2005. A simple empirical optical model for simulating light attenuation variability in a partially mixed estuary. Estuaries, 28, pp.572-580.

Zaneveld, J.R.V., Kitchen, J.C. and Pak, H., 1981. The influence of optical water type on the heating rate of a constant depth mixed layer. Journal of Geophysical Research: Oceans, 86(C7), pp.6426-6428.

Zhang, X., Marta-Almeida, M. and Hetland, R.D., 2012. A high-resolution pre-operational forecast model of circulation on the Texas-Louisiana continental shelf and slope. Journal of Operational Oceanography, 5(1), pp.19-34.

Zheng, L., Yang, Z., Lindley, C. and Myers III, E.P., 2020, December. NOAA/NOS Integrated Northern Gulf of Mexico Operational Forecast System. In AGU Fall Meeting Abstracts (Vol. 2020, pp. OS002-0009).

Zoffoli, M.L., Lee, Z., Ondrusek, M., Lin, J., Kovach, C., Wei, J. and Lewis, M., 2017. Estimation of transmittance of solar radiation in the visible domain based on remote sensing: Evaluation of models using in situ data. Journal of Geophysical Research: Oceans, 122(11), pp.9176-9188.

1141 Supplementary Materials

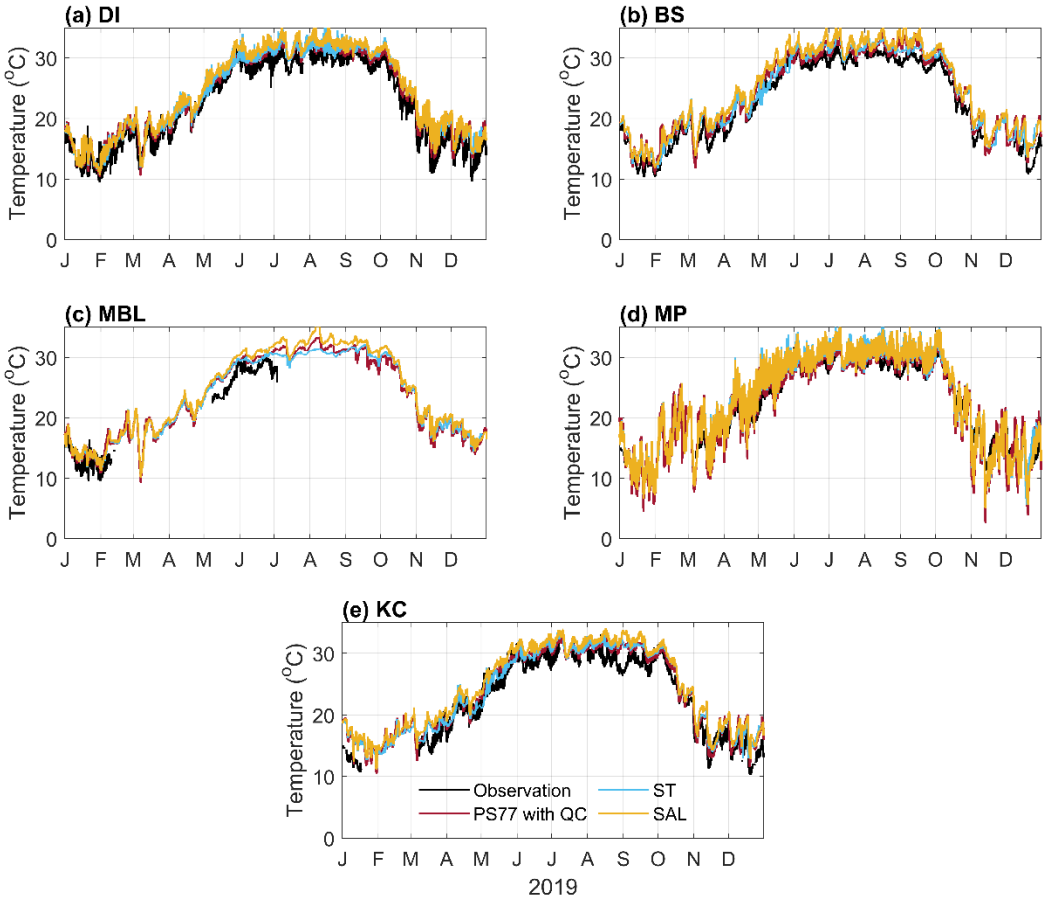

1142 Fig. S1. Comparison of observed and remaining modeled temperature time series during 2019 at
1143 five ARCOS stations.

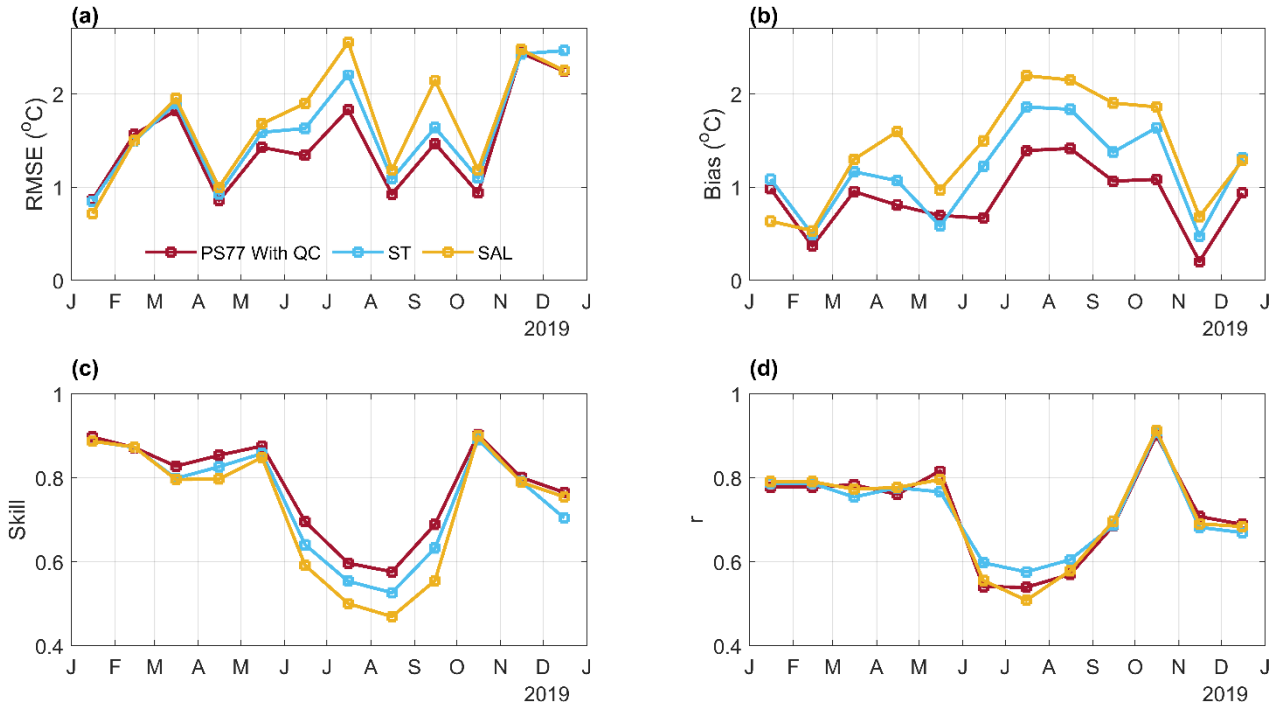

1144 Fig. S2. Remaining time-series comparison of monthly validation metrics between complied
1145 simulations and temperatures of five ARCOS stations during 2019.

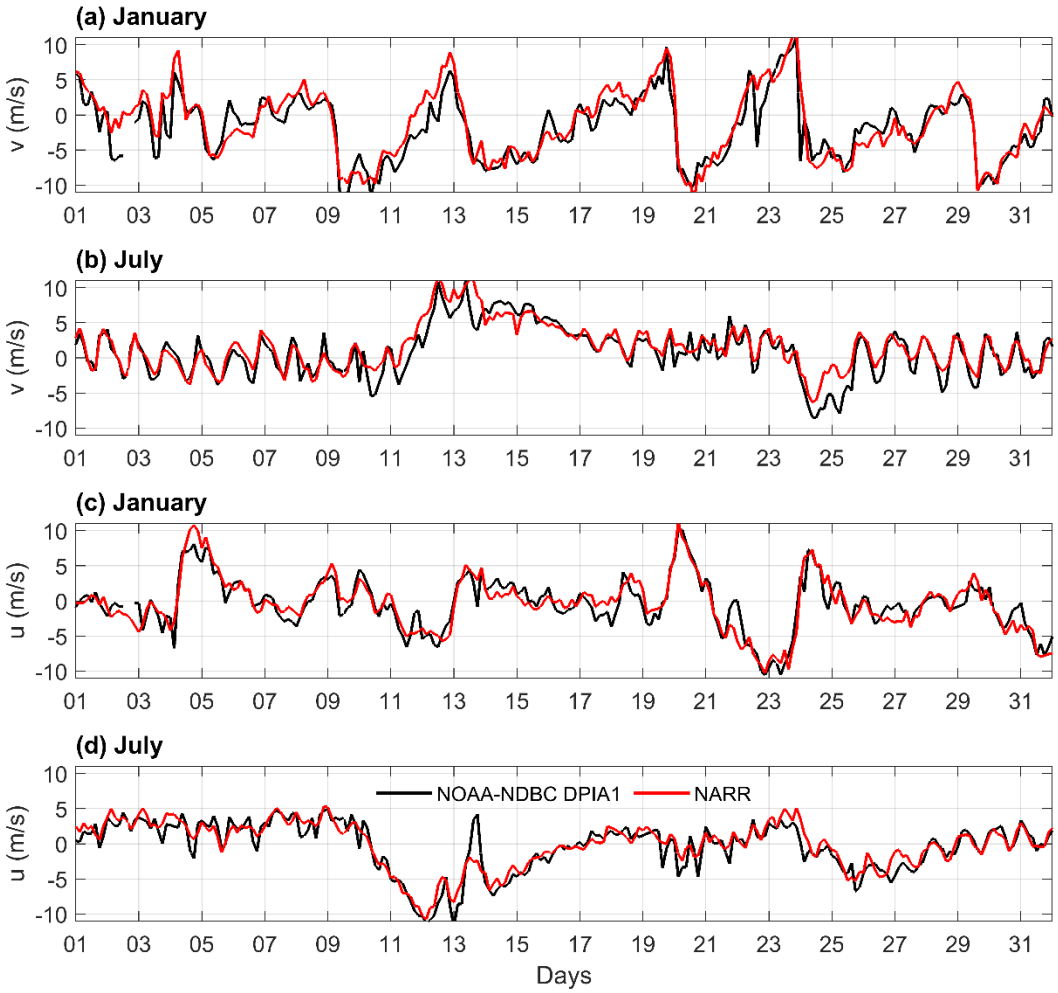

Fig. S3. Hourly averaged time series comparison of the NARR-derived u and v wind component (red) to corresponding DI NOAA (black) measurements during (a, c) January and (b, d) July. Positive values of *u* (*v*) indicate eastward (northward) wind, while negative values indicate westward (southward) wind.

Attenuation method	Dauphin Island (DI)				Bon Secour Bay (BS)			
	RMSE (°C)	Skill	Bias (°C)	r	RMSE (°C)	Skill	Bias (°C)	r
PS77	2.26	0.98	1.9	0.84	2.3	0.99	2.02	0.86
PS77 with QC	1.82	0.98	1.33	0.86	1.79	0.99	1.31	0.85
ST	2.73	0.97	1.46	0.82	2.46	0.98	1.16	0.85
ST with QC	3.23	0.95	0.59	0.65	1.32	0.99	0.6	0.75
SAL	2.41	0.97	1.89	0.84	2.15	0.97	1.84	0.87
SAL with QC	2.11	0.98	1.18	0.70	1.71	0.98	0.93	0.53

Attenuation method	Middle Bay Lighthouse (MBL)				Katrina Cut (KC)			
	RMSE (°C)	Skill	Bias (°C)	r	RMSE (°C)	Skill	Bias (°C)	r
PS77	1.22	0.99	0.54	0.89	2.32	0.99	1.76	0.92
PS77 with QC	1.07	0.99	0.44	0.9	1.83	0.99	1.13	0.91
ST	1.02	0.99	0.43	0.87	2.45	0.99	1.09	0.93
ST with QC	0.86	0.99	0.31	0.79	3.12	0.98	0.23	0.70
SAL	2.52	0.97	1.87	0.83	2.17	0.97	1.76	0.92
SAL with QC	2.28	0.98	1.49	0.75	1.83	0.98	0.93	0.75

Attenuation method	Meaher Park (MP)			
	RMSE (°C)	Skill	Bias (°C)	r
PS77	2.02	0.99	0.75	0.76
PS77 with QC	2.1	0.99	0.27	0.76
ST	2.5	0.99	0.47	0.74
ST with QC	3.4	0.98	-0.19	0.56
SAL	2.18	0.97	0.86	0.75
SAL with QC	2.59	0.96	0.14	0.55

Table S1. Statistical evaluation of temperatures simulated using six attenuation approaches with observations of five ARCOS stations during the year 2019.